Six years of continuous carbon isotope composition measurements of methane in Heidelberg (Germany) — a study of source contributions and comparison to emission inventories

Antje Hoheisel[1] and Martina Schmidt[1]

[1]Institute of Environmental Physics, Heidelberg University, Heidelberg, Germany

Correspondence: Antje Hoheisel (antje.hoheisel@iup.uni-heidelberg.de)

Abstract. ~~$\delta(^{13}CH_4)$~~ $\delta(^{13}C,CH_4)$ and the mole fraction of CH_4 have been measured continuously since April 2014 using a cavity ring-down spectroscopy (CRDS) analyser in Heidelberg, Germany. ~~This 6-year~~ Between 2014 and 2020, the time series shows an increasing trend of (6.8 ± 0.3) $nmol\,mol^{-1}\,a^{-1}$ for the CH_4 mole fraction ~~between 2014 and 2020. $\delta(^{13}CH_4)$~~ $\delta(^{13}C,CH_4)$ decreases by $(-0.028 \pm 0.002)\text{‰}\,a^{-1}$ over this time period.

In this study, seasonal variations and trends of CH_4 emissions in the catchment area of Heidelberg are analysed using three approaches by applying the ~~Miller-Tans~~ Keeling plot method to atmospheric measurements on different time scales. The mean ~~$\delta^{13}C$ isotopic~~ isotopic carbon source signature for the Heidelberg catchment area is ~~$(-52.5 \pm 0.3)\text{‰}$ (moving Miller-Tans~~ $(-52.3 \pm 0.3)\text{‰}$ (moving Keeling plot approach). In all three approaches, there is no significant trend in the monthly mean source signature over the last six years. However, more depleted source signature values occur in summer than in winter. This annual cycle in ~~^{13}C-CH_4 sources~~ the mean isotopic source signature, with a peak-to-peak amplitude of ~~-6.2‰~~ 5.8‰, can only be partially explained by seasonal variations in ~~CH_4~~ the ^{13}C-enriched emissions from heating. Additional seasonal variations probably occur in biogenic CH_4 emissions from waste water, landfills or dairy cows.

Furthermore, the source contributions derived from atmospheric measurements are used to evaluate the CH_4 emissions reported by two emission inventories: the Emissions Database for Global Atmospheric Research (EDGAR v6.0) and the inventory of the State Institute for the Environment Baden-Württemberg (LUBW - Landesanstalt für Umwelt Baden-Württemberg). The mean ~~$\delta(^{13}CH_4)$~~ $\delta(^{13}C,CH_4)$ source signature determined from the LUBW inventory agrees well with the result from atmospheric measurements. However, the signature determined from EDGAR v6.0 data is less depleted by about 7‰ compared to the results from atmospheric measurements. Thus, EDGAR v6.0 seems to overestimate CH_4 emissions from ~~more enriched~~ less depleted sources.

1 Introduction

One of the most challenging problems of our time is global warming. To limit the negative impacts associated with climate change, the 2015 UN Paris Agreement on Climate Change has set the goal to limit the mean global temperature increase to below 2 °C, preferably to 1.5 °C, compared to pre-industrial level (UNFCCC, 2015). In 2021 the United States, the European Union, and other countries launched the Global Methane Pledge with the goal to reduce global methane emissions. This

1

25 initiative recognised the short lifetime of methane (CH_4) of only 9.1 to 11.8 years (IPCC, 2021), allowing for a more rapid effect on atmospheric CH_4 mole fraction after reducing CH_4 emissions.

On a global scale several studies have analysed atmospheric carbon isotope ratios in methane, in addition to CH_4 mole fractions to constrain emission budgets and to explain observed atmospheric trends in mole fraction (e.g. Nisbet et.al, 2016, 2019; Schaefer, 2016, 2019 and Lan et al., 2021). This is possible, since each source type has a different isotopic signature depending 30 on the production processes and origin.

The isotopic composition of methane $\delta(^{13}C, CH_4)$, hereafter abbreviated as $\delta(^{13}CH_4)$, is described with the δ-notation, using the isotopic ratio R, and is typically given in ‰. The international reference standard for reporting $\delta(^{13}CH_4)$ is the Vienna Pee Dee Belemnite (VPDB; 0.0111802 ± 0.0000028, Werner and Brand 2001).

$$\delta = \frac{R_{sample}}{R_{standard}} - 1; \ R = \frac{^{13}CH_4}{^{12}CH_4} \tag{1}$$

35 CH_4 is emitted from anthropogenic and natural sources, which are grouped in three different categories according to the production processes. ~~Most depleted~~ Biogenic CH_4 ~~(−55‰ to −70‰) is specified as biogenic and is~~ is produced under anaerobic conditions due to degradation of organic matter ~~. Typical biogenic~~ (typically −70‰ to −55‰; IPCC, 2013). Biogenic CH_4 sources are wetlands, ruminants, landfills and wastewater treatment plants. Thermogenic CH_4, like that in natural gas, is formed on geological time scales out of organic matter and is ~~more enriched with values between −25‰ and −45‰. Most~~ 40 ~~enriched~~ less depleted than biogenic CH_4 ~~(−13‰~~ typically −45‰ to −25‰~~)~~; IPCC, 2013). Pyrogenic CH_4 is formed during the incomplete combustion of organic matter, such as biomass burning, and is ~~characterised as pyrogenic. (IPCC, 2013)~~ typically more enriched (typically −25‰ to −13‰; IPCC, 2013) compared to biogenic and thermogenic CH_4. Studies by Sherwood et al. (2017, 2021) and Menoud et al. (2022) show that $\delta(^{13}CH_4)$ of the different source categories are not always as distinct as indicated above. They give much larger ranges for the different source categories, which also overlap as a result. 45 Especially for fossil but also for biogenic sources large regional differences occur.

The knowledge of the spatial and temporal variation of CH_4 emissions around the world, and their composition from different types of sources, is important to reduce CH_4 emissions effectively and to understand the influence of different CH_4 sources on climate change. Also on a local and regional scale, the measurement of atmospheric ~~$\delta(^{13}C, CH_4)$, hereafter abbreviated as~~ $\delta(^{13}CH_4)$ ~~,~~ provides information about the contribution of different emission sectors to the total CH_4 emissions. Traditionally, 50 $\delta(^{13}CH_4)$ in the atmosphere is measured by collecting weekly flask or sample bags and analysing them with isotope ratio mass spectrometry (Miller et al., 2002; Fischer et al., 2006; Zazzeri et al., 2015; Röckmann et al., 2016). This method was used by Levin et al. (1999), who analysed and evaluated bi-weekly atmospheric samples in Heidelberg in the 1990s. With new measurement techniques such as continuous flow isotope ratio mass spectrometry (IRMS), quantum cascade laser absorption spectroscopy (QCLAS) or cavity ring-down spectroscopy (CRDS), the $\delta(^{13}CH_4)$ values in ambient air can be measured con- 55 tinuously and with high temporal resolutions from a few seconds up to minutes (Eyer et al., 2016; Röckmann et al., 2016; Hoheisel et al., 2019; Rennick et al., 2021).

There is a growing number of studies analysing atmospheric measurements of $\delta(^{13}CH_4)$ and of CH_4 mole fractions with high temporal resolution. Assan et al. (2018) analysed $\delta(^{13}CH_4)$ measurements near industrial sites and Röckmann et al.

(2016), as well as Menoud et al. (2020), studied $\delta(^{13}CH_4)$ in rural areas in the Netherlands. CH_4 measured at urban stations,
however, originates from heterogeneously distributed sources including waste management, natural gas distribution systems,
heating, transport and agriculture. The corresponding emissions vary strongly in their isotopic ^{13}C-CH_4 composition, and make
the analysis and interpretation of CH_4 emissions in cities more difficult (Menoud et al., 2021). However, isotope studies with
high-resolution measurements can also contribute to revealing possible inconsistencies in emission inventories in urban areas.
By analysing a 2-year time series of $\delta(^{13}CH_4)$ in London, Saboya et al. (2022) demonstrated that emissions from natural gas
leaks are underestimated in both the UK National Atmospheric Emissions Inventory (UK NAEI) and the Emissions Database
for Global Atmospheric Research (EDGAR).

At the urban station Heidelberg, the atmospheric CH_4 mole fraction and isotopic composition $\delta(^{13}CH_4)$ have been measured
continuously with a CRDS analyser since 2014. This measurement device enables the analysis of CH_4 and $\delta(^{13}CH_4)$ at high
temporal resolution of a few seconds. To our knowledge, our time series is the longest in situ $\delta(^{13}CH_4)$ record, with high
temporal resolution, reported to date. CH_4 emissions around Heidelberg originate from different sources due to the urban region
with rural surroundings. The regional emission inventory from the State Institute for the Environment Baden-Württemberg
(LUBW - Landesanstalt für Umwelt Baden-Württemberg) classified the CH_4 emissions for 2016 for the Heidelberg region to
the following main sectors: agriculture (30 %), waste management (30 %) and natural gas distribution systems (28 %) (LUBW,
2016).

In this study, a continuous six-year time series between 2014 and 2020 of the atmospheric CH_4 mole fraction and $\delta(^{13}CH_4)$
at the urban station Heidelberg is analysed to identify and understand seasonal and long-term variabilities of regional and
local CH_4 sources. Different approaches, such as the moving ~~Miller-Tans~~ Keeling plot approach, are used to determine the
contribution of different sectors to CH_4 total emissions in the catchment area of Heidelberg. These results are then compared to
a regional emission inventory provided by LUBW, and the emission database EDGAR v6.0. Thus, atmospheric measurements
are used to verify the estimated contribution of the different emission sectors to CH_4 emissions in the emission inventories.

2 Methods

2.1 Site description

Heidelberg ($\approx 159\,000$ inhabitants) is located in the south-west of Germany and in the north of the state Baden-Württemberg.
It is situated in the Upper Rhine Plain on the edge of the low mountain range Odenwald (Fig. 1). Therefore, the north-east is
less urban and more forested. More agricultural and urban areas are in the Upper Rhine Plain from the north-west to south-
east. The industrial cities of Mannheim ($\approx 312\,000$ inhabitants) and Ludwigshafen ($\approx 172\,000$ inhabitants) are $15\,km$ to $20\,km$
north-west of Heidelberg. Due to its location within industrial, urban, agricultural and rural areas, CH_4 emissions measured in
Heidelberg can originate from biogenic (e.g. dairy cows, waste water treatment plants), thermogenic (e.g. natural gas), and even
pyrogenic (e.g. traffic) sources. The CH_4 mole fraction and $\delta(^{13}CH_4)$ measurements are done at the Institute of Environmental
Physics (IUP - Institut für Umweltphysik, 49°25'2"N, 8°40'28"E, 116 m a.s.l.).

2.2 Experimental setup

Since April 2014, a cavity ring-down spectroscopy (CRDS) G2201-i analyser (Picarro, Inc., Santa Clara, CA) has been continuously measuring the dry air mole fraction of CH_4 and its $^{13}C/^{12}C$ ratio in ambient air with a temporal resolution of a few seconds. The intake for these ambient air measurements is located on the roof of the Institute for Environmental Physics (IUP-Institut für Umweltphysik) in Heidelberg, $30\,m$ above ground. Several studies have shown that the internal water correction, especially for $\delta(^{13}CH_4)$, is insufficient for this type of analyser (Rella et al., 2015; Hoheisel et al., 2019) and air drying is required for precise measurements. Thus, a cold trap cooled by a cryostat dries the air before it enters the CRDS analyser through a 16-way rotary valve (model: EMT2CSD16UWE, Valco Vici, Switzerland). The gas flow through the analyser is typically about $80\,ml\,min^{-1}$ and is monitored by an electronic flow meter (model: 5067-0223, Agilent Technologies, Inc., Santa Clara, CA). Every five hours, the ambient air measurement is interrupted to analyse calibration and quality control gases for 20 minutes each. The schematic of the laboratory setup is shown in Fig. 2.

2.3 Data treatment

The G2201-i analyser records CH_4 and the isotopic composition $\delta(^{13}CH_4)$ every $3.7\,s$. These high temporal resolution data are averaged to one-minute values. Before analysing these minutely CH_4 and $\delta(^{13}CH_4)$ values of ambient air, artefacts, outliers and invalid data are identified and flagged. These include periods of technical problems, work on the experimental setup such as replacing the cold trap, and the first five minutes after a change of sample gas to account for flushing of the cavity.

The one-minute CH_4 mole fractions and the isotopic composition of CH_4 are calibrated with a single-point calibration using the calibration measurements carried out every five hours. In August 2019, the calibration cylinder had to be replaced (see Table A1). The CH_4 mole fraction measurements are reported on the WMO X2004A scale (Dlugokencky et al., 2005) in $nmol\,mol^{-1} = 10^{-9}$ (nanomole per mole of dry air). The measurements of the isotopic compositions of CH_4 are traced to the Vienna Pee Dee Belemnite (VPDB) isotopic scale (Sperlich et al., 2016). Hence, in 2014 and 2019, the calibration cylinders were analysed with the gas chromatography (GC) system in Heidelberg (Levin et al., 1999) and the $\delta(^{13}CH_4)$ values were measured by the Stable Isotope Laboratory at Max Planck Institute for Biogeochemistry (MPI-BGC) in Jena.

2.4 Instrumental performance

The instrumental precision of the analyser was determined in 2013 and 2019 by performing measurements on different gas cylinders for at least $12\,h$ each. The Allan standard deviation determined from these measurements can be used as a measure of the repeatability of a measurement over a certain period of time. The Allan standard deviation of atmospheric CH_4 is below $0.11\,nmol\,mol^{-1}$ even for the high-resolution one-minute data. For an averaging interval of $15\,min$, corresponding to the calibration and target gas measurements, and CH_4 mole fractions between $1922\,nmol\,mol^{-1}$ and $2004\,nmol\,mol^{-1}$, the Allan standard deviation of CH_4 and $\delta(^{13}CH_4)$ is $0.08\,nmol\,mol^{-1}$ and $0.24‰$, respectively (see Fig. A1). The long-term reproducibility of the CRDS G2201-i analyser, i.e. the standard deviation of the target gas measurements performed between 2014 and 2020, is $0.2\,nmol\,mol^{-1}$ for CH_4 and $0.3‰$ for $\delta(^{13}CH_4)$ (see Fig. A2).

Six intercomparison cylinders with air samples from Neumayer Station in Antarctica were measured with our CRDS ~~G2201~~ G2201-i analyser to validate the measurement accuracy. These cylinders had already been analysed by the MPI-BGC within

125 the framework of an interlaboratory comparison (Umezawa et al., 2018). The average difference in $\delta(^{13}CH_4)$ between our results and the MPI-BGC measurements is $(0.02 \pm 0.05)‰$ (see Table A2).

3 Results and Discussion

3.1 Continuous CH_4 mole fraction and $\delta(^{13}CH_4)$ measurements

Atmospheric CH_4 mole fraction and $\delta(^{13}CH_4)$ were measured continuously with a CRDS analyser in Heidelberg between

130 April 2014 and May 2020. Figure 3 shows the daily mean CH_4 mole fractions, which vary between $1890\,\mathrm{nmol\,mol^{-1}}$ and $2310\,\mathrm{nmol\,mol^{-1}}$, with higher values in winter than in summer. The corresponding isotopic composition $\delta(^{13}CH_4)$ ranges from ~~$-49‰$ to $-47‰$~~ $-49.3‰$ to $-47.3‰$.

The digital filter curve fitting ~~programme~~ program CCGCRV[1] developed by Kirk Thoning (Earth System Group, Earth System Laboratory (CCG/ESRL), NOAA, Thoning et al. 1989) is applied to the monthly average data to analyse the trend and

135 annual cycle of CH_4 and $\delta(^{13}CH_4)$. CCGCRV can be used to decompose a time series into a trend and a detrended seasonal cycle by fitting a polynomial equation combined with a harmonic function to the data and applying a filter to the residuals. In this study, we used 3 polynomial terms and 4 annual harmonic terms. The short- and long-term cutoff values for the low-pass filter are 80 and 667, respectively. Between 2014 and 2020, the CH_4 mole fraction increases by $(6.8 \pm 0.3)\,\mathrm{nmol\,mol^{-1}\,a^{-1}}$ and $\delta(^{13}CH_4)$ shows a decreasing trend of $(-0.028 \pm 0.002)‰\,\mathrm{a^{-1}}$. Furthermore, CH_4 and $\delta(^{13}CH_4)$ show strong mean annual

140 cycles (right panel of Fig. 3). The maximum of the mean CH_4 mole fraction occurs in late autumn (November). In winter and spring, the mole fraction decreases slightly until it reaches a minimum in late summer (June to July). The amplitude (peak-to-peak height) is $78\,\mathrm{nmol\,mol^{-1}}$ in CH_4. The annual cycle in atmospheric $\delta(^{13}CH_4)$ has a mean amplitude of $0.4‰$. ~~Less enriched $\delta(^{13}CH_4)$ values of $-48.3‰$ occur in~~ In early autumn (September to October) ~~, with the most enriched values of $-47.9‰$~~ the $\delta(^{13}CH_4)$ values are more depleted than the values in spring (April to May).

145 In addition to the trend and the annual cycle, the CH_4 mole fraction and $\delta(^{13}CH_4)$ show diurnal variations. The mean diurnal cycles for different seasons are presented in Fig. 4. In the afternoon (15-16 UTC), the overnight increase in the CH_4 mole fraction begins due to the lower mixing height. After sunrise, the mole fraction decreases strongly due to radiation-induced mixing and thus an increase of the mixing height. The mean diurnal cycles show strong seasonal differences with larger variations in summer ($52\,\mathrm{nmol\,mol^{-1}}$) and weaker ones in winter ($21\,\mathrm{nmol\,mol^{-1}}$). Since the diurnal cycle is strongly

150 driven by the sun, the earlier sunrise and later sunset in summer compared to winter is additionally noticeable by the earlier decrease of CH_4 in the morning and the later increase in the afternoon. The diurnal variations of $\delta(^{13}CH_4)$ show slightly larger amplitudes in summer ($0.18‰$) and autumn ($0.16‰$) than in winter ($0.09‰$) and spring ($0.12‰$). The lowest $\delta(^{13}CH_4)$ values

---

[1]CCGCRV: https://www.esrl.noaa.gov/gmd/ccgg/mbl/crvfit/index.html and ftp://ftp.cmdl.noaa.gov/user/thoning/ccgcrv/

occur around 7 to 10 UTC. $\delta(^{13}CH_4)$ increases during the day to maximum values between 18 and 21 UTC, before decreasing at night. It seems that in summer, the depletion in $\delta(^{13}CH_4)$ in the morning is slightly stronger than in the other seasons.

3.2 Comparison of $\delta(^{13}CH_4)$ with background and former measurements

In Heidelberg, the CH_4 mole fraction and $\delta(^{13}CH_4)$ were measured with a GC- IRMS system and from bi-weekly integral flask samples between 1992 and 1997 (Levin et al., 1999). Since the previous CH_4 mole fractions were reported on the CMDL83 scale, we take into account that the CH_4 mole fractions measured on the new WMO 2004 scale are a factor of (1.0124 ± 0.0007) larger (Dlugokencky et al., 2005). Figure 5 shows CH_4 and $\delta(^{13}CH_4)$ from the two time periods (1992-1998, 2014-2020) for which $\delta(^{13}CH_4)$ measurements were done in Heidelberg. In addition to the Heidelberg measurements, monthly data from the marine background station Mace Head Observatory (Lan et al., 2022; Michel et al., 2022) are shown. The Mace Head Observatory (53°19'36"N, 9°54'16"E, 8.4 m a.s.l.) is located on the west-coast of Ireland and measures the maritime background mole fraction when air is coming from the ocean. The isotopic composition measured at Mace Head by the Institute of Arctic and Alpine Research (INSTAAR) of the University of Colorado has to be subtracted by an offset of $0.28‰$ to take into account the inter-comparison offset among the laboratories INSTAAR and MPI-BGC (Umezawa et al., 2018).

Again the curve fitting program CCGCRV is applied to the monthly mean values to determine trends and seasonal variabilities. The observed increasing trend in Heidelberg between April 2014 and June 2020 is only slightly smaller than the one in Mace Head. This is was different in the 1990s, where the CH_4 mole fraction did not follow the increasing trend observed at the background station Izaña (Levin et al., 1999) or Mace Head. Furthermore, the continental CH_4 excess at Heidelberg (Heidelberg data minus Mace Head data) strongly decreased between the 1990s and recent years (2014-2020) to $(70 \pm 3)\,\mathrm{nmol\,mol^{-1}}$, which is only half of the value from the 1990s. These observations can be explained by a change in the emission rate in the catchment area of Heidelberg. In the studies by Levin et al. (2011, 2021) the CH_4 fluxes in the catchment area of Heidelberg are calculated with the Radon-Tracer method. They found a $30\,\%$ reduction of CH_4 emissions between 1996 and 2004 and no further systematic trend thereafter. In the 1990s, the $\delta(^{13}CH_4)$ values in Heidelberg decreased strongly with $-0.14‰\,\mathrm{a^{-1}}$, while samples from Izaña only show trends which are more than a factor of three smaller (Levin et al., 1999). This difference in the $\delta(^{13}CH_4)$ trends points to a change in the composition of CH_4 emissions in the catchment area of Heidelberg. Levin et al. (1999) attribute this change to a reduction of CH_4 emissions from fossil sources (mainly coal mining) and from cattle breeding. The situation is different for recent measurements (2014 to 2020). The current Heidelberg data only show a small trend in $\delta(^{13}CH_4)$ which is similar to the one observed at Mace Head. Therefore, the CH_4 source mixture in the catchment area of Heidelberg seems to be relatively constant during the last years.

3.3 Isotopic carbon signature of CH_4 sources calculated with atmospheric measurements

CH_4 sources contributing to the atmospheric CH_4 mole fraction have different $\delta^{13}C$ isotopic isotopic carbon source signatures depending on their origin and production process. These isotopic source signatures can range from $-13‰$ to $-70‰$ (Sherwood et al., 2021; Menoud et al., 2022). Therefore, the measured atmospheric $\delta(^{13}CH_4)$ value strongly depends on the CH_4 source mixture from regional and local sources. That makes it possible to analyse the CH_4 sources in the Heidelberg catchment

based on the measured atmospheric CH_4 mole fraction in combination with the observed atmospheric isotopic composition $\delta(^{13}CH_4)$. In most cases, an increase in atmospheric CH_4 mole fraction will be caused by a mixture of CH_4 emitted from different sources. Thus, from the atmospheric measurements, one usually does not obtain information about a single source, but the average isotopic signature of several contributing sources depending on their respective emission rate.

3.3.1 Determination of mean ~~$\delta^{13}C$~~ isotopic carbon source signatures

In this study we use the ~~Miller-Tans method (Miller and Tans, 2003)~~ Keeling plot method (Keeling, 1958, 1961) in combination with the York fit (York et al., 2004) to determine the mean ~~$\delta^{13}C$ isotopic~~ isotopic carbon source signature in the catchment area of Heidelberg. This method is applied to the one-minute averages of CH_4 and $\delta(^{13}CH_4)$ for which the Allan standard deviation is used as a measure of instrumental uncertainty. The ~~Miller-Tans~~ Keeling plot method uses the linear relationship between ~~$\delta_{obs} \cdot C_{obs}$ and C_{obs}~~ δ_{obs} and $1/C_{obs}$, where C and δ refer to CH_4 and $\delta(^{13}CH_4)$:

$$\delta_{obs} = \frac{1}{C_{obs}} \cdot \underline{C_{obs} = C_{bg} \cdot (\delta_{bg} - \delta_s) + \delta_s \cdot C_{obs}}. \tag{2}$$

Here, the indices ~~obs, bg and s~~ obs, bg and s denote observed, background and source values. The York fit was chosen as this method minimises the weighted distance between the data points and the fitted line, taking into account uncertainties in both x and y-coordinates. ~~Tests have shown that for our application there is no difference between the Miller-Tans or the Keeling plot (Keeling, 1958, 1961) methods when using the York fit. The compatibility of these methods was also shown by Zobitz et al. (2006) for CO_2 and Hoheisel et al. (2019) for CH_4. The~~

The uncertainty of the source signature determined with the ~~Miller-Tans~~ Keeling plot method and the York fit strongly depends on the precision of the analyser and the peak height of CH_4 ~~above background~~ (Hoheisel et al., 2019). To achieve accurate results for the mean ~~$\delta^{13}C$ isotopic~~ isotopic carbon source signatures, we apply two criteria to our data: the CH_4 range of the dataset, to which the Keeling plot is applied, has to be larger than $100 \, nmol \, mol^{-1}$ and the fit error on the slope of the regression line has to be smaller than $2.5‰$.

Another method to determine the mean isotopic carbon source signature is derived by Miller and Tans (2003). For comparison, we also determined the mean isotopic source signatures of CH_4 with the Miller-Tans method (Miller and Tans, 2003, Equation 5), which uses the linear relationship between $\delta_{obs} \cdot C_{obs}$ and C_{obs}, and where the background values can remain unknown:

$$\delta_{obs} \cdot C_{obs} = C_{bg} \cdot (\delta_{bg} - \delta_s) + \delta_s \cdot C_{obs}. \tag{3}$$

In our case, there is no difference between the Keeling plot and the Miller-Tans method, when using the York fit. The compatibility of these methods was also shown by Zobitz et al. (2006) for CO_2 and Hoheisel et al. (2019) for CH_4.

Different approaches are tested for the choice of time scale (month, night, ~~event~~ moving interval) for which the mean ~~$\delta^{13}C$ isotopic~~ isotopic carbon source signature for Heidelberg should be calculated. Depending on the time scale, the ~~Miller-Tans~~ Keeling plot method is applied to different data subsets (each month, each night, moving interval). Larger time intervals of one month have the advantage that the CH_4 mole fractions cover a large range, which increases the precision of the results of the regression line. On the other hand, uncertainties occur since the background is probably not constant over the entire time period,

which can be assumed for shorter time intervals of a few hours. The three most promising approaches used in this study are the monthly, the night-time and the moving ~~Miller-Tans~~ Keeling plot approach. In the monthly approach, the ~~Miller-Tans~~ Keeling plot method is applied to the one-minute average data of each month of each year. In the night-time approach, the ~~Miller-Tans~~ Keeling plot method is applied to the one-minute average data between 17 and 7 CET. This approach uses the night-time increase in the CH_4 mole fraction caused by the accumulation of CH_4 emissions in the lower boundary layer. Therefore, we determine the mean ~~$\delta^{13}C$ isotopic~~ isotopic carbon source signature of the contributing CH_4 sources for each night. In order to achieve meaningful results, only nocturnal data sets that fulfil our two criteria (CH_4 range $>100\,\mathrm{nmol\,mol^{-1}}$, regression fit error for the slope $<2.5\%o$) are used. This is the case for 21% of the night data sets. We can therefore determine the mean ~~$\delta^{13}C$ isotopic~~ isotopic carbon source signature in the catchment area of Heidelberg for 460 nights.

Due to the high temporal resolution of our CH_4 mole fraction and $\delta(^{13}CH_4)$ measurements, we can go one step further and determine the ~~$\delta^{13}C$ isotopic source signatures of events~~ isotopic carbon source signatures with a moving ~~Miller-Tans~~ Keeling plot approach similar to the moving Keeling plot or moving Miller-Tans methods used by Röckmann et al. (2016), Menoud et al. (2020), Assan et al. (2018) or Saboya et al. (2022). Since we are interested in short-term events, a time window with a fixed length of one hour is shifted over the one-minute average data set with time steps of one minute. Thus, for each minute t_i, the mean ~~$\delta^{13}C$ isotopic~~ isotopic carbon source signature is calculated from a one-hour time period centred on t_i using the ~~Miller-Tans~~ Keeling plot method and the York fit. Again only those results which fulfil our two criteria of a CH_4 range larger than $100\,\mathrm{nmol\,mol^{-1}}$ during the time window and a fit error of the slope smaller than $2.5\%o$ are used. If these criteria for t_i are not achieved, the result for t_i calculated with a time window one hour longer is used. This continues until both criteria are fulfilled or the length of the time window reaches 12 hours. If the criteria are still not met for the 12 hours time interval, the result is excluded. With the moving ~~Miller-Tans~~ Keeling plot approach, we achieve results for 18% of the one-minute average data. To take into account that several of the mean isotopic source signatures determined for each minute may describe the same event, an average is taken over ~~all values directly adjacent in time. Thus, the mean $\delta^{13}C$ isotopic source signatures of 769 events are determined for the six years between April 2011 and May 2020.~~ each hour.

3.3.2 Monthly averages and annual cycle of the mean ~~$\delta^{13}C$~~ isotopic carbon source signatures

Figure 6a shows the monthly averaged values of the mean ~~$\delta^{13}C$ isotopic~~ isotopic carbon signatures of the CH_4 sources in the Heidelberg catchment area, which were determined using the monthly (black), night-time (blue) and moving ~~Miller-Tans~~ Keeling plot (red) approaches. The monthly mean ~~$\delta^{13}C$ isotopic~~ isotopic carbon source signatures vary between $-61.5\%o$ and $-42.3\%o$ and show similar results for the three different approaches. The average mean ~~$\delta^{13}C$ isotopic~~ isotopic carbon source signature of CH_4 in Heidelberg for the whole time period of six years is ~~$(-52.5 \pm 0.3)\%o$~~ $(-52.3 \pm 0.3)\%o$ (mean$\pm$standard error of the mean), calculated with the moving ~~Miller-Tans~~ Keeling plot approach. The result from the night-time approach is $(-52.3 \pm 0.4)\%o$ and does not differ significantly from the moving ~~Miller-Tans~~ Keeling plot approach. The result from the monthly approach is $(-53.9 \pm 0.3)\%o$ and is only slightly ~~less enriched~~ more depleted than the results from the other two approaches. Thus, the average mean isotopic source signature of CH_4 is more depleted than the mean $\delta(^{13}CH_4)$ value in the atmosphere in Heidelberg $(-48.07 \pm 0.02)\%o$. ~~This indicates~~

Since the determined mean isotopic source signature is low and close to what could be expected if biogenic sources (typically between $-55‰$ and $-70‰$) were dominant, a strong influence from biogenic CH_4 sources, such as waste management and agriculture, in the catchment area of Heidelberg ~~.~~ can be assumed.

255   In comparison, the mean isotopic source signatures determined for two five month measurement campaigns in more rural areas in the Netherlands, where ruminants are a main CH_4 source, were $(-60.8 \pm 0.2)‰$ (Röckmann et al., 2016) and $(-59.55 \pm 0.13)‰$ (Menoud et al., 2020). Looking at other studies in urban areas, Menoud et al. (2021) reported an overall source signature of $-48.7‰$ in Krakow (Poland, 6-month campaign), and Saboya et al. (2022) calculated a median isotopic source signature of $-41.6‰$ for London (UK, 2.7 years), indicating that the primary CH_4 sources in London are natural

260   gas leaks. The mean ~~$\delta^{13}C$ isotope signature~~ isotopic carbon signature of CH_4 in Heidelberg thus shows a contribution from ~~enriched~~ less ^{13}C depleted sources such as natural gas, heating, and even traffic from the Heidelberg urban area in addition to biogenic emissions. However, neither of these sources appear to be the only main emitter. This is consistent with the emission inventory of the State Institute for the Environment Baden-Württemberg (LUBW, 2016) for the Heidelbeg area, which reports one third of the emissions each from natural gas leakage, the waste sector, or agriculture (see Fig. 8 in section 3.4.1).

265   Between 2014 and 2020, no significant trend is detectable in the monthly mean ~~$\delta^{13}C$ isotopic~~ isotopic carbon source signatures obtained from all three approaches. Therefore, we assume that the general composition of CH_4 emissions in the Heidelberg catchment area has not changed or has changed only slightly during this period. This finding is different to a former study by Levin et al. (1999) from the 1990s. They found a change in the $\delta(^{13}CH_4)$ source signature from $(-47.4 \pm 1.2)‰$ in 1992/1993 to $(-52.9 \pm 0.4)‰$ in 1995/1996 and attribute this change to a reduction of CH_4 emissions from fossil sources

270   (mainly coal mining) and from cattle breeding.

Moreover, a commonality between the mean ~~$\delta^{13}C$ isotopic~~ isotopic carbon source signatures calculated with the different approaches is that a strong annual cycle with more depleted values in the summer than in the winter months can be noticed (Fig. 6b). The annual cycles calculated with all three approaches show most depleted source signatures in June. From June to October the ~~$\delta^{13}C$ isotopic~~ isotopic carbon source signatures increase ~~to more enriched values~~ and stay relatively constant

275   until April. Between April and June a strong decrease ~~to more depleted values~~ in the mean isotopic carbon source signature is visible. This annual cycle clearly indicates that in summer the CH_4 emissions have a larger biogenic share compared to the rest of the year. When analysing each year individually, the majority have a detectable annual cycle, and it is therefore a very well-defined signal that does not arise from one or two very pronounced annual cycles.

3.3.3   Mean ~~$\delta^{13}C$~~ isotopic carbon source signatures of individual nights and ~~events~~ days

280   An advantage of the night-time and moving ~~Miller-Tans~~ Keeling plot approach compared to the monthly approach is that the mean ~~$\delta^{13}C$ isotopic~~ isotopic carbon source signature of individual nights or ~~events~~ days can be studied. Figure 7a shows the histogram of the mean ~~$\delta^{13}C$ isotopic~~ isotopic carbon source signatures of 460 individual nights calculated with the night-time approach, and Figure 7b displays a similar histogram using the mean ~~$\delta^{13}C$ isotopic source signatures for the 769 events~~ isotopic carbon source signatures averaged for each day determined by the moving ~~Miller-Tans~~ Keeling plot approach. Most of

285   the CH_4 emissions during one night or ~~event~~ day are a mixture from several sources and cannot be attributed to one particular

source. When separating the night-time and ~~event~~ day source signatures into winter/spring (Nov to Apr) and summer/autumn (May to Oct), a shift in the mean ~~δ^{13}C isotopic~~ isotopic carbon source signature of approximately ~~2.5‰~~ 2‰ is noticeable. ~~More depleted mean δ^{13}C isotopic~~ The mean isotopic carbon source signatures of (-53.5 ± 0.4)‰ or ~~(-53.6 ± 0.3)‰ occur~~ (-53.2 ± 0.2)‰ in summer/autumn ~~and more enriched~~ is less depleted than the ones of (-51.1 ± 0.5)‰ or ~~(-51.0 ± 0.4)‰~~ (-51.3 ± 0.3)‰ in winter/spring for the night-time or the moving ~~Miller-Tans~~ Keeling plot approach, respectively (Fig. 7). This annual cycle is also described in section 3.3.2. Both approaches additionally have in common that our criteria are fulfilled for fewer nights or ~~events~~ days in winter than in summer. Only 41% to 43% of the determined ~~δ^{13}C isotopic~~ isotopic carbon source signatures occur between Nov and Apr. Since the diurnal variations are usually lower in winter than in summer, more night-time increases ~~or events~~ have ranges below the chosen threshold of $100\,\mathrm{nmol\,mol^{-1}}$ and are therefore excluded.

Furthermore, we determined the diurnal cycle for the mean ~~δ^{13}C isotopic~~ isotopic carbon source signatures calculated with the moving ~~Miller-Tans~~ Keeling plot approach. However, the year to year variations are too strong compared to the possible mean diurnal cycle to get reliable results and to exclude the possibility that the noticeable diurnal variations are only an artefact of the averaging. Even though we can analyse the ~~δ^{13}C isotopic~~ isotopic carbon source signature at time scales below individual months, the precision of our analyser is still too low to interpret diurnal variations. ~~Although~~ However, the development of new instruments with better precision of isotope measurements will soon make this possible.

3.3.4 Discussion of different approaches

The average mean ~~δ^{13}C isotopic~~ isotopic carbon source signatures of CH_4 and the annual cycles in Heidelberg calculated with the moving ~~Miller-Tans~~ Keeling plot approach or the night-time approach from the whole six-year time period show no significant differences. This ~~indicates~~ can indicate that the composition of CH_4 sources in Heidelberg is the same during day and night or that the emissions during the night-time increase contribute most in the moving ~~Miller-Tans approach, too~~ Keeling plot approach.

The monthly approach results in similar monthly mean ~~δ^{13}C isotopic~~ isotopic carbon source signatures and a similar annual cycle to the other two approaches. The average mean source signature is, however, approximately ~~1.4‰ less enriched~~ 1.6‰ more depleted than the results from the moving ~~Miller-Tans~~ Keeling plot and the night-time approaches (Fig. 6a). The reason for this difference cannot be conclusively resolved in this study. One possibility is that this difference can be caused by the assumption of a constant background over the entire month~~or the fact that all one-minute average data points of the month contribute to the determined source signature. In the night-time and the Miller-Tans approaches nights and time periods which do not fulfil our criteria are discarded, which can exclude small pollution events. As all data points are used in the monthly approach, the small events also contribute to the mean δ^{13}C isotopic source signature. Another explanation can be, that the considered~~ . Another explanation is that the CH_4 emissions considered in the monthly, night-time and moving ~~Miller-Tans~~ Keeling plot approaches represent different catchment areas ~~. CH_4 emissions from more distant sources show lower and more temporally extended CH_4 peaks in the measured time series than emissions from local and regional sources. In the analysis of small time intervals of several hours, more distant emissions can be excluded by the selection criteria. Thus, the night-time and moving Miller-Tans approach probably consider more distant emissions less often than local and regional ones. Furthermore,~~

320 ~~at~~ and sources, which may cause the difference in the average mean isotopic source signatures. At night, the footprint of Heidelberg is smaller than during the day. In 2018, around 47% of the surface influence calculated with the Stochastic Time-Inverted Lagrangian Transport (STILT) model (Lin et al., 2003 and Kountouris et al., 2018) for the station Heidelberg is within $50\,km$ at night (time of the day: 18 to 3), but within $100\,km$ during the day (time of the day: 6 to 15). For these calculations the STILT footprint tools[2] and the STILT jupyter notebook service[3] were used. Thus, the monthly approach, which includes

325 daytime data, represents a larger catchment area than the night-time approach. Furthermore, CH_4 emissions from more distant sources show lower and more temporally extended CH_4 peaks in the measured time series than emissions from local and regional sources. In the analysis of small time intervals of several hours, more distant emissions can be excluded by the selection criteria. Thus, the night-time and moving Keeling plot approach probably consider more distant emissions less often than local and regional ones. Excluding nights and time periods that do not fulfil our criteria can of course exclude small pollution events

330 in the night-time and Miller-Tans approach regardless of the distance of the source. These small pollution events, however, contribute to the mean isotopic carbon source signature in the monthly approach, since all one-minute average data points are used there.

Different CH_4 sources have different isotopic source signatures, which depend on the production process of CH_4. The isotopic source signatures of several sources in the surroundings of Heidelberg are characterised in Hoheisel et al. (2019). Biogenic

335 CH_4 emitted from livestock, landfills, and wastewater treatment is more depleted ~~. Thermogenic~~ compared to thermogenic CH_4 from the gas distribution system ~~is less depleted~~ (see Table 1). Other studies such as Levin et al. (1999), Menoud et al. (2021), and Zazzeri et al. (2017) report isotopic source signatures from combustion processes for traffic, industry, and energy for buildings (see Table 1). This pyrogenic CH_4 is even less depleted than thermogenic CH_4. Since the measurement site in Heidelberg is located in an urban area, the nearby CH_4 sources are more often natural gas leaks, ~~wastewater,~~ traffic, or emissions from

340 energy for buildings. ~~These CH_4 emissions are on average less depleted.~~ The more distant sources tend to be in rural areas, so that emissions from landfills and livestock are more prominent. ~~These biogenic emissions are more depleted~~ Therefore, the nearby CH_4 emissions are on average less depleted, than the more distant biogenic emissions. This agrees well with the more depleted mean ~~$\delta^{13}C$ isotopic~~ isotopic carbon source signature of CH_4 calculated with the monthly approach, in comparison to the night-time approach.

345 We tested the robustness of the monthly, night-time and moving ~~Miller-Tans~~ Keeling plot approaches by varying the selection criteria. The CH_4 range was set to be $100\,nmol\,mol^{-1}$, $150\,nmol\,mol^{-1}$ or $200\,nmol\,mol^{-1}$, and the threshold for the fit error of the slope was changed from $2.5\permil$ over $5\permil$ to $10\permil$. All determined monthly mean source signatures show similar results, with an annual cycle containing more biogenic values in summer. The monthly ~~values vary on average~~ mean isotopic source signatures calculated with different selection criteria show differences between $0.1\permil$ and $0.8\permil$, with standard deviations

350 between $1\permil$ and $3\permil$. Therefore, we choose the CH_4 range of $100\,nmol\,mol^{-1}$ as threshold to include more data sets and $2.5\permil$ as threshold for the fit error of the slope, and thus the uncertainty of the source signature, to still assure precise results.

---

[2]STILT footprint tools: https://www.icos-cp.eu/data-services/tools/stilt-footprint

[3]STILT jupyter notebook service: https://www.icos-cp.eu/data-services/tools/jupyter-notebook

Furthermore, several automatic approaches to identify the nocturnal increases for each night in the time series were tested. The determined monthly averaged ~~δ^{13}C isotopic~~ isotopic carbon source signatures did not vary strongly between the automatic approaches and the one using the fixed time window. Since the automatic approaches did not correctly identify the CH$_4$ increase

355 for all nights, we chose the same fixed time interval between 17 and 7 CET for the nightly increase of CH$_4$ for each day. Also, varying the fixed time interval does not lead to any relevant changes in the monthly averaged mean ~~δ^{13}C isotopic~~ isotopic carbon source signatures. In addition, we tested a more common method for the moving ~~Miller-Tans~~ Keeling plot approach starting with a 12 hours time window. Then the time interval is reduced in hourly steps when our two criteria are not fulfilled. There is no significant difference between the monthly averaged mean ~~δ^{13}C isotopic~~ isotopic carbon source signatures of the

360 two moving ~~Miller-Tans~~ Keeling plot scenarios.

To conclude, all three approaches have their advantages depending on the temporal and spatial range we are interested in. We have shown that the monthly approach is a good and easy solution to determine the monthly mean source signature and deviates only slightly from the more specific night-time and moving ~~Miller-Tans~~ Keeling plot approach. Especially for remote stations which only observe small diurnal variations in CH$_4$ this method is a good option, when night-time and moving ~~Miller-Tans~~

365 Keeling plot approaches struggle with the low variations. We tested the monthly approach at the mountain station Schauinsland (~~1205~~ 47°54'50" N, 7°54'28" E, 1205 m a.s.l.) operated by the German Environment Agency (UBA - Umweltbundesamt) to determine the mean ~~δ^{13}C isotopic~~ isotopic carbon signature of CH$_4$ for two measurement campaigns of one month. In the summer campaign (Sep to Oct 2018) the mean source signature is (-60.3 ± 0.7)‰ and in the winter campaign (Feb to Mar 2019) (-56.9 ± 0.4)‰. The larger influence of biogenic emissions in summer can also be seen at the Schauinsland station.

370 ## 3.4 Comparison of CH$_4$ source contribution with different emission inventories

Emission inventories are based on bottom-up methods which involve statistical data about emitters, such as animal population or the amount and type of combusted fuel, and specific emission factors that quantify the emissions from different source categories (IPCC, 2006). Both, statistical data and emission factors, can have large uncertainties, for instance, due to unknown and unaccounted sources or high spatial and temporal variability. In addition to national emission inventories, regional emission

375 inventories for each county are reported on a yearly basis, for example by the State Institute for the Environment Baden-Württemberg (LUBW, 2016). Other emission inventories, such as the Emissions Database for Global Atmospheric Research (EDGARv6.0, Crippa et al., 2021), ~~go one step further~~ extend the effort and aim to provide accurate annual emissions for different source types covering the entire globe. The different emission inventories can show, though, strong deviations in the amount and composition of emissions for the same area. Therefore, it is important to verify the reported greenhouse gas

380 emissions given by emission inventories on a global, a national as well as a regional scale. Only then can the intended reduction of greenhouse gases be confirmed and, if necessary, the mitigation strategy adapted.

In this study, the measurements of the atmospheric CH$_4$ mole fraction and the isotopic composition $\delta(^{13}$CH$_4)$ were used to calculate a mean ~~δ^{13}C isotopic~~ isotopic carbon source signature and its annual cycle for the catchment area of Heidelberg (Sect. 3.3). In the following section, these results are compared to two different emission inventories to constrain their estimated

385 emissions and to explain the noticed annual cycle in the mean ~~δ^{13}C isotopic~~ isotopic carbon source signature determined for
the catchment area of Heidelberg.

3.4.1 Emission inventories

The first emission inventory used in this study is provided by the State Institute for the Environment Baden-Württemberg
(LUBW, 2016) and the second is the Emissions Database for Global Atmospheric Research (EDGAR v6.0, Crippa et al.,
390 2021). Since the measurements in Heidelberg were carried out at low elevation about $30\,\mathrm{m}$ above ground and within the city,
the atmospheric CH_4 mole fraction measurements are most strongly influenced by local and regional sources. The LUBW
provides detailed information about CH_4 emissions depending on different CH_4 categories for the cities of Heidelberg (HD)
and Mannheim (MA), the county Rhein-Neckar-Kreis (RNK), and the state Baden-Württemberg (BW) for the reference year
2016 (see Fig. 8).
395   EDGAR v6.0[4] estimates CH_4 emissions from different categories for $0.1° \times 0.1°$ grid cells covering the whole world. In
addition to annual sector-specific gridmaps, monthly sector-specific gridmaps are also provided for the years 2000 to 2018.

Emissions for the Heidelberg, Mannheim, and Rhein-Neckar-Kreis areas are determined from the monthly sector-specific
gridmaps using all grid cells which are at least partly within the borders of the respective county. Thereby, the emissions from
each cell are weighted in the summation according to the percentage of overlap between the cell and the county and are then
400 added up for each year. The CH_4 emissions provided by EDGAR v6.0 for the years 2014 to 2018 vary between $12731\,\mathrm{t a^{-1}}$ and
$13685\,\mathrm{t a^{-1}}$ in the Heidelberg area (including HD, MA and RNK), and seem to decrease slightly by $7\,\%$. The average emission
for the whole time period is $(13319 \pm 163)\,\mathrm{t a^{-1}}$.

Figure 8 shows the emissions for the Heidelberg area per section for LUBW (2016) and EDGAR (2014-2018). The sectors
which contribute most are natural gas, waste treatment and livestock farming. For the Heidelberg area (HD,MA,RNK) the
405 average emissions determined by EDGAR v6.0 are 3.4 times larger than CH_4 emissions provided by LUBW ($3915\,\mathrm{t a^{-1}}$). Both
inventories report comparable CH_4 emissions from livestock farming (1.1 times larger emissions by EDGAR v6.0 than LUBW),
but strong differences occur for emissions from the waste treatment and waste incineration sector (3.5 times), the natural gas
sector (4.9 times) and the energy for buildings sector (4.5 times). EDGAR v6.0 reports CH_4 emissions from waste incineration,
which are comparable to the emissions from waste water treatment plants. These emissions are not reported separately by the
410 LUBW.

The city of Mannheim forms a connected urban area with the city of Ludwigshafen and is only separated by the river
Rhine. Several industrial companies such as BASF are located there, especially near the river. In the EDGAR v6.0 inventory,
strong CH_4 emissions occur in the two grid cells on the border between Mannheim and Ludwigshafen for the industry, gas,
oil and waste treatment sectors. Thus, CH_4 emissions determined from the EDGAR v6.0 inventory for Mannheim can include
415 emissions from Ludwigshafen. In these grid cells, CH_4 emissions from waste treatment or the power industry sector can be
assigned primarily to sites in Mannheim. However, the emissions from combustion for the manufacturing sector as well as the
natural gas and oil sector cannot be separated so easily and could therefore lead to larger differences to the LUBW inventory.

---

[4]EDGAR v6.0: https://edgar.jrc.ec.europa.eu/index.php/dataset_ghg60

Unfortunately, to our knowledge, there is no sector-separated CH_4 inventory for Ludwigshafen that could be included in the LUBW inventory. However, the distribution of emissions at the border of the areas cannot explain the whole deviation. Indeed, the CH_4 emissions for all of Baden-Württemberg are still 1.5 times larger in EDGAR v6.0 than reported by LUBW. Again strong differences occur for the waste treatment and waste incineration sector (4.0 times larger emissions by EDGAR v6.0 than LUBW) as well as the energy for buildings sector (3.9 times).

The differences between the reported CH_4 emissions by EDGAR v6.0 and LUBW are probably partly caused by differences in the statistical data, especially by different assumptions for the emission factors used to estimate the CH_4 emissions from different sectors. This is supported by the fact that the amount of emissions from sectors ~~, such as livestock farming,~~ with well studied emission factors and accurate statistical data are comparable for both inventories, such as livestock farming. CH_4 emissions estimated by EDGAR v5.0 for Germany have an uncertainty of only 16% for the agriculture sector, while the uncertainty for the waste sector is 43% (Solazzo et al., 2021). These values are estimated for the CH_4 emissions of Germany. The uncertainty of individual or several grid cells can be even larger. The LUBW does not report uncertainties of the CH_4 emissions.

3.5 ~~Mean δ^{13}C isotopic signature of CH_4 sources in the Heidelberg area~~

3.4.1 Mean isotopic carbon signature of CH_4 sources in the Heidelberg area

The two emission inventories of LUBW and EDGAR v6.0 report CH_4 emissions depending on source sectors. By attributing a source specific ~~δ^{13}C isotopic~~ isotopic carbon signature to the emissions of each sector, the mean ~~δ^{13}C isotopic~~ isotopic carbon signature of CH_4 sources in the Heidelberg area can be determined. The isotopic signatures for each source sector are chosen, if possible, from results of measurement campaigns in the catchment area of Heidelberg (Hoheisel et al., 2019, Levin et al., 1993). Table 1 summarises the ~~δ^{13}C isotopic~~ isotopic carbon source signatures used for the different sectors. Despite intensive literature research we have not been able to find any publications describing δ^{13}C for CH_4 emitted by waste incineration. ~~in the way we needed them to calculate the mean δ^{13}C isotopic source signature.~~ Thus, we adopted the ^{13}C composition of waste incineration reported by Widory et al. (2006) for CO_2. This is possible, since no strong isotopic fractionation is noticeable during the combustion for CO_2 and we assume that no strong fractionation of ^{13}C occurs for CH_4, either.

The mean ~~δ^{13}C isotopic~~ isotopic carbon source signature for the Heidelberg area determined using the LUBW (2016) inventory is $-52\permil$. The result calculated from the average EDGAR v6.0 data for the years 2014 to 2018 for the Heidelberg area is $-46\permil$. The uncertainty of the determined source signatures is $2\permil$ and it is calculated from the variations in the ~~δ^{13}C isotopic~~ isotopic carbon signatures of the emission sectors. Since no uncertainties are reported for the CH_4 emissions in the LUBW inventory or the grid cells in the EDGAR v6.0 inventory, their impact on the determined mean source signature could not be taken into account.

A large difference of $6\permil$ between the mean source signature determined from LUBW and EDGAR v6.0 data occurs and is caused by the differences in the relative source mixture. On the right side in Fig. 8, the relative amount of CH_4 emissions per sector is shown for the Heidelberg area. Biogenic CH_4, which is ~~most depleted~~ typically more depleted compared

14

to thermogenic or pyrogenic CH_4, contributes most in the LUBW inventory from livestock farming and waste treatment giving 30% each. In the EDGAR v6.0 inventory, only 10% and 22% of anthropogenic CH_4 is emitted by livestock farming and waste treatment in the Heidelberg area. At the same time, much more thermogenic and even pyrogenic CH_4, which is ~~more enriched~~less depleted than biogenic CH_4, is emitted in the EDGAR v6.0 (2014-2018) inventory compared to the LUBW inventory. In the EDGAR v6.0 (2014-2018) inventory, 41% of anthropogenic CH_4 is emitted from the natural gas sector and 9% from waste incineration. The LUBW inventory reports only 28% of anthropogenic CH_4 from the natural gas sector and does not include emissions from waste incineration.

3.5 ~~Comparison between mean $\delta^{13}C$ isotopic source signatures calculated with atmospheric measurements and emission inventories~~

~~The mean $\delta^{13}C$ isotopic~~

3.4.1 Comparison between mean isotopic carbon source signatures calculated with atmospheric measurements and emission inventories

The mean isotopic carbon source signatures calculated for the LUBW and EDGAR v6.0 inventories are compared to the mean isotopic source signature determined out of atmospheric measurements. The annual mean isotopic carbon signature determined using EDGAR v6.0, $(-46 \pm 2)\%_0$, is approximately $7\%_0$ less depleted than the results from atmospheric measurements calculated with the moving Keeling plot, $(-52.3 \pm 0.3)\%_0$, or the night-time approach. The results from the LUBW inventory, $(-52 \pm 2)\%_0$, show similar values to the mean source signatures determined out of atmospheric measurements, with only a small difference of less than $1\%_0$.

Figure 9 shows the ~~mean $\delta^{13}C$ isotopic source signatures for each month and the annual averages (dashed lines)~~annual averages of the mean isotopic carbon source signatures, which are determined out of atmospheric measurements (black) or using the EDGAR v6.0 ~~inventory~~ (blue) ~~. The dashed redline displays the annual mean source signature calculated with the LUBW inventory. The monthly values shown as solid red line are determined using the annual LUBW data, including~~ and LUBW (red) inventories, as dashed lines. In addition, the mean isotopic carbon source signatures for each month are displayed (solid lines). EDGAR v6.0 reports monthly CH_4 emissions, which were used to calculate the monthly mean isotopic carbon source signatures. The most prominent annual cycle in the CH_4 emissions estimated by EDGAR v6.0 occurs in the energy for buildings sector. The LUBW only reports annual emissions. Therefore, we included a modelled annual cycle for the ~~sector~~ energy for buildings sector (the LUBW sector small and medium-sized combustion plants ~~(~~ KuMF). This modelled annual cycle is based on the ~~most prominent annual cycle in the CH_4 emissions estimated by~~ annual cycle noticeable in the monthly EDGAR v6.0 ~~: the one~~ emissions for the energy for ~~building~~ buildings sector.

The ~~annual mean $\delta^{13}C$ isotopic signatures determined using~~ monthly mean isotopic source signatures calculated using the EDGAR v6.0 ~~are approximately $7\%_0$ more enriched than the results from atmospheric measurements calculated with the moving Miller-Tans approach. The results from the LUBW inventory show similar values to the mean source signatures determined out of atmospheric measurements, with only a small difference of less than $1\%_0$. Furthermore, mean source~~

~~signatures calculated using the two~~ and the LUBW inventories also show an annual cycle with more depleted values in summer compared to winter. However, the peak-to-peak amplitude in the annual cycle determined out of atmospheric measurements is ~~6.2~~5.8‰ and thus approximately three times larger than the annual cycles noticeable by EDGAR v6.0 and the modelled LUBW data. Thus, the observed annual cycle resulting from atmospheric measurements can only be partly explained by seasonal variations of CH_4 emissions from heating. This indicates that emissions from another sector have relevant seasonal variations too, which are not yet included into EDGARv6.0 inventory.

By using inverse models, Bergamaschi et al. (2018) found an annual cycle in CH_4 emissions in Germany, with the maximum in summer. Due to the limited number of studies, they could not quantitatively estimate potential seasonal variations of anthropogenic sources (Bergamaschi et al., 2018). However, some studies such as Ulyatt et al. (2010), Spokas et al. (2011) and VanderZaag et al. (2014) reported an annual cycle in CH_4 emissions from biogenic sources such as dairy cows, landfills or waste water with more emissions in summer. Such seasonal variations in biogenic emissions, in addition to the variations of emissions from heating, can explain the annual cycle in the catchment area of Heidelberg determined by atmospheric measurements.

The comparison between the isotopic carbon signatures determined using emissions from the EDGAR v6.0 inventory and the results from atmospheric measurements indicates that EDGAR v6.0 seems to overestimate CH_4 emissions from less depleted sources in the catchment area of Heidelberg. A recent study with mobile CH_4 measurements in Heidelberg by Wietzel and Schmidt (2023) show that the EDGAR 6.0 and the LUBW emission inventories most probably overestimate the emissions from natural gas distribution systems in the city of Heidelberg. When comparing our results with studies in other cities, it becomes clear that the representativeness of emissions inventories can strongly vary by region and city. Saboya et al. (2022) showed that the mean isotopic source signature in EDGAR v4.3.2 for London is approximately -12‰ lower than the median of the isotopic source signatures, indicating that emissions due to natural gas leaks in London are being underestimated. Menoud et al. (2021) found that the average isotopic source signatures from the model using the EDGAR v5.0 inventory in Krakow are in good agreement with the ones from the measurements. These differences in the studies show the importance and significance of regional and local studies using continuous isotope measurements.

4   Conclusion

In this study, the continuous time series of atmospheric CH_4 and $\delta(^{13}CH_4)$ measured over six years in Heidelberg is used to study seasonal variations and trends of CH_4 emissions in the catchment area of Heidelberg. The CH_4 mole fraction increases by $(6.8 \pm 0.3)\,\mathrm{nmol\,mol^{-1}\,a^{-1}}$ between 2014 and 2020 and $\delta(^{13}CH_4)$ shows a decreasing trend of (-0.028 ± 0.002)‰ $\mathrm{a^{-1}}$. Furthermore, CH_4 and $\delta(^{13}CH_4)$ show strong annual cycles with the minimum in late summer and early autumn, respectively.

The partitioning of local and regional CH_4 emissions among different source categories is analysed by determining the mean ~~$\delta^{13}C$ isotopic~~ isotopic carbon source signature in the catchment area of Heidelberg. Therefore, the ~~Miller-Tans~~ Keeling plot method in combination with the York fit are applied to the measured atmospheric CH_4 and $\delta(^{13}CH_4)$ time series. Three different approaches are tested which correspond to different time intervals: the monthly approach, the night-time approach

and the moving ~~Miller-Tans~~ Keeling plot approach. In all these approaches, no significant trend in the monthly mean source signature occurs during the last six years. This confirms that the source composition in the catchment area of Heidelberg did not change between 2014 and 2020.

520   The average mean source ~~signatures calculated with the above described approaches vary between -52.3‰ and -53.9‰~~ signature calculated with night-time and the moving Keeling plot approaches is (-52.3 ± 0.4)‰. The CH_4 emissions measured in Heidelberg originate from different sources in the urban area as well as in the rural surroundings. They range from biogenic sources, such as livestock over waste treatment, to thermogenic sources, such as natural gas, and even to pyrogenic ones, such as traffic and wood-firing installations. The determined monthly mean ~~$\delta^{13}C$ isotopic~~ isotopic carbon source signatures of all

525 approaches show an annual cycle with a peak-to-peak amplitude of ~~6.2‰~~ 5.8‰ and a stronger biogenic CH_4 contribution in summer. The comparison with emission inventories have shown that this cycle can only be partly explained by seasonal variations in the CH_4 emissions from heating. Thus, additional seasonal variations probably occur in biogenic CH_4 emissions from waste water, landfills or dairy cows. However, there is still a great need for research in order to understand and describe potential annual cycles of CH_4 sources precisely.

530   Furthermore, the mean ~~$\delta^{13}C$ isotopic~~ isotopic carbon source signatures determined for the catchment area of Heidelberg using atmospheric measurements are used to verify the CH_4 emissions reported by two emission inventories. EDGAR v6.0 seems to overestimate CH_4 emissions from ~~more enriched~~ less depleted sources. The mean source signature resulting from EDGAR v6.0 data is around 7‰ ~~more enriched~~ less depleted than the one determined from atmospheric measurements. This large difference can be partly explained by the large amount of CH_4 emissions estimated by EDGAR v6.0 for waste incineration

535 and the energy for buildings sector. The LUBW inventory estimates much lower CH_4 emissions than EDGAR v6.0, especially for the waste sector. The mean ~~$\delta^{13}C$ isotopic~~ isotopic carbon source signature calculated using the emissions reported by LUBW agrees well with the result from atmospheric measurements. This study gives a first impression about how well the emission inventories represent the CH_4 emissions in the catchment area of Heidelberg.

References

Assan, S., Vogel, F. R., Gros, V., Baudic, A., Staufer, J., and Ciais, P.: Can we separate industrial CH4 emission sources from atmospheric observations? - A test case for carbon isotopes, PMF and enhanced APCA, Atmos. Environ., 187, 317-327, https://doi.org/10.1016/j.atmosenv.2018.05.004, 2018.

Bergamaschi, P., Karstens, U., Manning, A. J., Saunois, M., Tsuruta, A., Berchet, A., Vermeulen, A. T., Arnold, T., Janssens-Maenhout, G., Hammer, S., Levin, I., Schmidt, M., Ramonet, M., Lopez, M., Lavric, J., Aalto, T., Chen, H. L., Feist, D. G., Gerbig, C., Haszpra, L., Hermansen, O., Manca, G., Moncrieff, J., Meinhardt, F., Necki, J., Galkowski, M., O'Doherty, S., Paramonova, N., Scheeren, H. A., Steinbacher, M., and Dlugokencky, E.: Inverse modelling of European CH4 emissions during 2006-2012 using different inverse models and reassessed atmospheric observations, Atmos. Chem. Phys., 18, 901-920, https://doi.org/10.5194/acp-18-901-2018, 2018.

Crippa, Monica; Guizzardi, Diego; Muntean, Marilena; Schaaf, Edwin; Lo Vullo, Eleonora; Solazzo, Efisio; Monforti-Ferrario, Fabio; Olivier, Jos; Vignati, Elisabetta: EDGAR v6.0 Greenhouse Gas Emissions. European Commission, Joint Research Centre (JRC) [Dataset] PID: http://data.europa.eu/89h/97a67d67-c62e-4826-b873-9d972c4f670b, 2021.

Dlugokencky, E. J., Myers, R. C., Lang, P. M., Masarie, K. A., Crotwell, A. M., Thoning, K. W., Hall, B. D., Elkins, J. W., and Steele, L. P.: Conversion of NOAA atmospheric dry air CH$_4$ mole fractions to a gravimetrically prepared standard scale, J. Geophys. Res.-Atmos., 110, 8, https://doi.org/10.1029/2005jd006035, 2005.

Dlugokencky, E. J., Crotwell, A. M., Mund, J. W., Crotwell, M. J. and Thoning, K. W., Atmospheric Methane Dry Air Mole Fractions from the NOAA GML Carbon Cycle Cooperative Global Air Sampling Network, 1983-2019, Version: 2020-07, https://doi.org/10.15138/VNCZ-M766, 2020.

Eyer, S., Tuzson, B., Popa, M. E., van der Veen, C., Röckmann, T., Rothe, M., Brand, W. A., Fisher, R., Lowry, D., Nisbet, E. G., Brennwald, M. S., Harris, E., Zellweger, C., Emmenegger, L., Fischer, H., and Mohn, J.: Real-time analysis of δ^{13}C- and δDCH$_4$ in ambient air with laser spectroscopy: method development and first intercomparison results, Atmos. Meas. Tech., 9, 263– 280, https://doi.org/10.5194/amt-9-263-2016, 2016.

Fisher, R., Lowry, D., Wilkin, O., Sriskantharajah, S., Nisbet, E.G.: High-precision, automated stable isotope analysis of atmospheric methane and carbon dioxide using continuous-flow isotope-ratio mass spectrometry, Rapid Commun. Mass Spectrom. 20, 200e208, https://doi.org/10.1002/rcm.2300, 2006.

Hoheisel, A., Yeman, C., Dinger, F., Eckhardt, H., and Schmidt, M.: An improved method for mobile characterisation of δ^{13}CH$_4$ source signatures and its application in Germany, Atmos. Meas. Tech., 12, 1123-1139, https://doi.org/10.5194/amt-12-1123-2019, 2019.

IPCC (2006): IPCC Guidelines for National Greenhouse Gas Inventories, Prepared by the National Greenhouse Gas Inventories Programme, edited by: Eggleston, H. S., Buendia, L., Miwa, K., Ngara, T., and Tanabe, K., Institute for Global Environmental Strategies, Japan, 2006.

IPCC (2013): Climate Change 2013: The Physical Science Basis. Contribution of Working Group I to the Fifth Assessment Report of the Intergovernmental Panel on Climate Change, edited by: Stocker, T.F., D. Qin, G.-K. Plattner, M. Tignor, S.K. Allen, J. Boschung, A. Nauels, Y. Xia, V. Bex and P.M. Midgley, Cambridge University Press, Cambridge, United Kingdom and New York, NY, USA, 1535 pp, 2013.

IPCC (2021): Climate Change 2021: The Physical Science Basis. Contribution of Working Group I to the Sixth Assessment Report of the Intergovernmental Panel on Climate Change, edited by: Masson-Delmotte, V., P. Zhai, A. Pirani, S.L. Connors, C. Péan, S. Berger, N. Caud, Y. Chen, L. Goldfarb, M.I. Gomis, M. Huang, K. Leitzell, E. Lonnoy, J.B.R. Matthews, T.K. Maycock, T. Waterfield, O. Yelekçi, R.

Yu, and B. Zhou, Cambridge University Press, Cambridge, United Kingdom and New York, NY, USA, In press, https://doi.org/10.1017/9781009157896.

Keeling, C. D.: The concentration and isotopic abundances of atmospheric carbon dioxide in rural areas, Geochim. Cosmochim. Acta, 13, 322-334, https://doi.org/10.1016/0016-7037(58)90033-4, 1958.

590   Keeling, C. D.: The concentration and isotopic abundances of carbon dioxide in rural and marine air. Geochim. Cosmochim. Acta. 24, 277–298, https://doi.org/10.1016/0016-7037(61)90023-0, 1961.

Kountouris, P., Gerbig, C., Rödenbeck, C., Karstens, U., Frank Koch, T. and Heimann, M.: Technical Note: Atmospheric CO2 inversions on the mesoscale using data-driven prior uncertainties: Methodology and system evaluation, Atmos. Chem. Phys., 18(4), 3027–3045, https://doi.org/10.5194/acp-18-3027-2018, 2018.

595   Lan, X., Basu, S., Schwietzke, S., Bruhwiler, L. M. P., Dlugokencky, E. J., Michel, S. E., Sherwood, O. A., Tans, P. P., Thoning, K., Etiope, G., Zhuang, Q., Liu, L., Oh, Y., Miller, J. B., Pétron, G., Vaughn, B. H., and Crippa, M.: Improved Constraints on Global Methane Emissions and Sinks Using δ^{13}C-CH$_4$, Global Biogeochem. Cy., 35, 007000, https://doi.org/10.1029/2021GB007000, 2021.

Lan, X., Dlugokencky, E.J., Mund, J.W., Crotwell, A.M., Crotwell, M.J., Moglia, E., Madronich, M., Neff, D., and Thoning, K.W.: Atmospheric Methane Dry Air Mole Fractions from the NOAA GML Carbon Cycle Cooperative Global Air Sampling Network, 1983-2021,
600   Version: 2022-11-21, https://doi.org/10.15138/VNCZ-M766, 2022.

Levin, I., Atmosphärisches CO2, Quellen und Senken auf dem Europäischen Kontinent, PhD thesis, University of Heidelberg, Germany, 1984.

Levin, I., Bergamaschi, P., Dörr, H., and Trapp, D.: Stable isotopic signature of methane from major sources in Germany, Chemosphere, 26, 161-177, https://doi.org/10.1016/0045-6535(93)90419-6, 1993.

605   Levin, I., Glatzel-Mattheier, H., Marik, T., Cuntz, M., Schmidt, M., and Worthy, D. E.: Verification of German methane emission inventories and their recent changes based on atmospheric observations, J. Geophys. Res.-Atmos., 104, 3447-3456, https://doi.org/10.1029/1998jd100064, 1999.

Levin, I., Hammer, S., Eichelmann, E. and Vogel F. R.: Verification of greenhouse gas emission reductions: the prospect of atmospheric monitoring in polluted areas Phil. Trans. R. Soc. A.3691906–1924, http://doi.org/10.1098/rsta.2010.0249, 2011.

610   Levin, I., Karstens, U., Hammer, S., DellaColetta, J., Maier, F., and Gachkivskyi, M.: Limitations of the radon tracer method (RTM) to estimate regional greenhouse gas (GHG) emissions – a case study for methane in Heidelberg, Atmos. Chem. Phys., 21, 17907–17926, https://doi.org/10.5194/acp-21-17907-2021, 2021.

Lin, J. C., Gerbig, C., Wofsy, S. C., Andrews, A. E., Daube, B. C., Davis, K. J. and Grainger, C. A.: A near-field tool for simulating the upstream influence of atmospheric observations: The Stochastic Time-Inverted Lagrangian Transport (STILT) model, J. Geophys. Res. D
615   Atmos., 108(16), https://doi.org/10.1029/2002JD003161, 2003.

LUBW - Landesanstalt für Umwelt Baden-Württemberg: https://www.lubw.baden-wuerttemberg.de/luft/kataster and personal communication with M. Vogel and T. Leiber from LUBW in April and December 2019.

Menoud, M., van der Veen, C., Scheeren, B., Chen, H., Szénási, B., Morales, R. P., Pison, I., Bousquet, P., Brunner, D., and Röckmann, T.: Characterisation of methane sources in Lutjewad, The Netherlands, using quasi-continuous isotopic composition measurements, Tellus B:
620   Chemical and Physical Meteorology, 72, 1-20, https://doi.org/10.1080/16000889.2020.1823733, 2020.

Menoud, M., van der Veen, C., Necki, J., Bartyzel, J., Szénási, B., Stanisavljević, M., Pison, I., Bousquet, P., and Röckmann, T.: Methane (CH4) sources in Krakow, Poland: insights from isotope analysis, Atmos. Chem. Phys., 21, 13167–13185, https://doi.org/10.5194/acp-21-13167-2021, 2021.

Menoud, M., van der Veen, C., Lowry, D., Fernandez, J. M., Bakkaloglu, S., France, J. L., Fisher, R. E., Maazallahi, H., Stanisavljević, M., Nęcki, J., Vinkovic, K., Łakomiec, P., Rinne, J., Korbeń, P., Schmidt, M., Defratyka, S., Yver-Kwok, C., Andersen, T., Chen, H., and Röckmann, T.: New contributions of measurements in Europe to the global inventory of the stable isotopic composition of methane, Earth Syst. Sci. Data, 14, 4365–4386, https://doi.org/10.5194/essd-14-4365-2022, 2022.

Michel, S.E., Clark, J.R., Vaughn, B.H., Crotwell, M., Madronich, M., Moglia, E., Neff, D., Mund, J.: Stable Isotopic Composition of Atmospheric Methane (13C) from the NOAA GML Carbon Cycle Cooperative Global Air Sampling Network, 1998-202, University of Colorado, Institute of Arctic and Alpine Research (INSTAAR), Version: 2022-12-15 https://doi.org/10.15138/9p89-1x02, 2022.

Miller, J. B., Mack, K. A., Dissly, R., White, J. W., Dlugokencky, E. J., and Tans, P. P.: Development of analytical methods and measurements of $^{13}C/^{12}C$ in atmospheric CH_4 from the NOAA Climate Monitoring and Diagnostics Laboratory Global Air Sampling Network, Journal of Geophysical Research, 107(D13), 4178, https://doi.org/10.1029/2001JD000630, 2002.

Miller, J. B., and Tans, P. P.: Calculating isotopic fractionation from atmospheric measurements at various scales, Tellus Ser. B-Chem. Phys. Meteorol., 55, 207-214, https://doi.org/10.1034/j.1600-0889.2003.00020.x, 2003.

Nisbet, E. G., Dlugokencky, E. J., Manning, M. R., Lowry, D., Fisher, R. E., France, J. L., Michel, S. E., Miller, J. B., White, J. W. C., Vaughn, B., Bousquet, P., Pyle, J. A., Warwick, N. J., Cain, M., Brownlow, R., Zazzeri, G., Lanoiselle, M., Manning, A. C., Gloor, E., Worthy, D. E. J., Brunke, E. G., Labuschagne, C., Wolff, E. W., and Ganesan, A. L.: Rising atmospheric methane: 2007-2014 growth and isotopic shift, Glob. Biogeochem. Cycle, 30, 1356-1370, https://doi.org/10.1002/2016gb005406, 2016.

Nisbet, E. G., Manning, M. R., Dlugokencky, E. J., Fisher, R. E., Lowry, D., Michel, S. E., Myhre, C. L., Platt, M., Allen, G., Bousquet, P., Brownlow, R., Cain, M., France, J. L., Hermansen, O., Hossaini, R., Jones, A. E., Levin, I., Manning, A. C., Myhre, G., Pyle, J. A., Vaughn, B. H., Warwick, N. J., and White, J. W. C.: Very Strong. Atmospheric Methane Growth in the 4 Years 2014-2017: Implications for the paris Agreement, Glob. Biogeochem. Cycle, 33, 318-342, https://doi.org/10.1029/2018gb006009, 2019.

Rella, C. W., Hoffnagle, J., He, Y., and Tajima, S.: Local- and regional-scale measurements of CH_4, $\delta^{13}CH_4$, and C_2H_6 in the Uintah Basin using a mobile stable isotope analyzer, Atmos. Meas. Tech., 8, 4539-4559, https://doi.org/10.5194/amt-8-4539-2015, 2015.

Rennick, C., Arnold, T., Safi, E., Drinkwater, A., Dylag, C., Webber, E. M., Hill-Pearce, R., Worton, D.R., Bausi, F. and Lowry, D.: Boreas: A sample preparation-coupled laser spectrometer system for simultaneous high-precision in situ analysis of $\delta13C$ and $\delta2H$ from ambient air methane. Analytical Chemistry, 93(29), 10141–10151. https://doi.org/10.1021/acs.analchem.1c01103, 2021.

Röckmann, T., Eyer, S., van der Veen, C., Popa, M. E., Tuzson, B., Monteil, G., Houweling, S., Harris, E., Brunner, D., Fischer, H., Zazzeri, G., Lowry, D., Nisbet, E. G., Brand, W. A., Necki, J. M., Emmenegger, L., and Mohn, J.: In situ observations of the isotopic composition of methane at the Cabauw tall tower site, Atmos. Chem. Phys., 16, 10469-10487, https://doi.org/10.5194/acp-16-10469-2016, 2016.

Saboya, E., Zazzeri, G., Graven, H., Manning, A. J., and Englund Michel, S.: Continuous CH_4 and $\delta^{13}CH_4$ measurements in London demonstrate under-reported natural gas leakage, Atmos. Chem. Phys., 22, 3595–3613, https://doi.org/10.5194/acp-22-3595-2022, 2022.

Schaefer, H., Fletcher, S. E. M., Veidt, C., Lassey, K. R., Brailsford, G. W., Bromley, T. M., Dlugokencky, E. J., Michel, S. E., Miller, J. B., Levin, I., Lowe, D. C., Martin, R. J., Vaughn, B. H., and White, J. W. C.: A 21st-century shift from fossil-fuel to biogenic methane emissions indicated by (CH4)-C-13, Science, 352, 80-84, https://doi.org/10.1126/science.aad2705, 2016.

Schaefer, H.: On the Causes and Consequences of Recent Trends in Atmospheric Methane, Curr. Clim. Chang. Rep., 5, 259-274, https://doi.org/10.1007/s40641-019-00140-z, 2019.

Sherwood, O. A., Schwietzke, S., Arling, V. A., and Etiope, G.: Global Inventory of Gas Geochemistry Data from Fossil Fuel, Microbial and Burning Sources, version 2017, Earth Syst. Sci. Data, 9, 639-656, https://doi.org/10.5194/essd-9-639-2017, 2017.

Sherwood, O. A., Schwietzke, S., and Lan, X.: Global δ13C-CH4 Source Signature Inventory 2020, Earth System Research Laboratories, https://doi.org/10.15138/qn55-e011, 2021.

Solazzo, E., Crippa, M., Guizzardi, D., Muntean, M., Choulga, M., and Janssens-Maenhout, G.: Uncertainties in the Emissions Database for Global Atmospheric Research (EDGAR) emission inventory of greenhouse gases, Atmos. Chem. Phys., 21, 5655–5683, https://doi.org/ 10.5194/acp-21-5655-2021, 2021.

Sperlich, P., Uitslag, N. A. M., Richter, J. M., Rothe, M., Geilmann, H., van der Veen, C., Röckmann, T., Blunier, T., and Brand, W. A.: Development and evaluation of a suite of isotope reference gases for methane in air, Atmos. Meas. Tech., 9, 3717-3737, https://doi.org/10.5194/amt-9-3717-2016, 2016.

Spokas, K., Bogner, J., and Chanton, J.: A process-based inventory model for landfill CH4 emissions inclusive of seasonal soil microclimate and CH4 oxidation, J. Geophys. Res.-Biogeosci., 116, 19, https://doi.org/10.1029/2011jg001741, 2011.

Thoning, K. W., Tans, P. P., and Komhyr, W. D.: ATMOSPHERIC CARBON-DIOXIDE AT MAUNA LOA OBSERVATORY .2. ANALYSIS OF THE NOAA GMCC DATA, 1974-1985, J. Geophys. Res.-Atmos., 94, 8549-8565, https://doi.org/10.1029/JD094iD06p08549, 1989.

Ulyatt, M. J., Lassey, K. R., Shelton, I. D., and Walker, C. F.: Seasonal variation in methane emission from dairy cows and breeding ewes grazing ryegrass/white clover pasture in New Zealand, New Zeal. J. Agr. Res., 45, 217–226, https://doi.org/10.1080/00288233.2002. 9513512, 2010.

Umezawa, T., Brenninkmeijer, C. A. M., Röckmann, T., van der Veen, C., Tyler, S. C., Fujita, R., Morimoto, S., Aoki, S., Sowers, T., Schmitt, J., Bock, M., Beck, J., Fischer, H., Michel, S. E., Vaughn, B. H., Miller, J. B., White, J. W. C., Brailsford, G., Schaefer, H., Sperlich, P., Brand, W. A., Rothe, M., Blunier, T., Lowry, D., Fisher, R. E., Nisbet, E. G., Rice, A. L., Bergamaschi, P., Veidt, C., and Levin, I.: Interlaboratory comparison of δ13C and δD measurements of atmospheric CH4 for combined use of data sets from different laboratories, Atmos. Meas. Tech., 11, 1207–1231, https://doi.org/10.5194/amt-11-1207-2018, 2018.

UNFCCC (2015): The Paris Agreement. United Nations Framework Convention on Climate Change. Retrieved from http://unfccc.int/paris_ agreement/items/9485.php, 2015.

VanderZaag, A. C., Flesch, T. K., Desjardins, R. L., Balde, H., and Wright, T.: Measuring methane emissions from two dairy farms: Seasonal and manure-management effects, Agric. For. Meteorol., 194, 259-267, https://doi.org/10.1016/j.agrformet.2014.02.003, 2014.

Werner, R. A., and Brand, W. A.: Referencing strategies and techniques in stable isotope ratio analysis, Rapid Commun. Mass Spectrom., 15, 501-519, https://doi.org/10.1002/rcm.258, 2001.

White, J. W. C., Vaughn, B. H. and Michel, S. E.: Stable Isotopic Composition of Atmospheric Methane (13C) from the NOAA ESRL Carbon Cycle Cooperative Global Air Sampling Network, 1998-2017, University of Colorado, Institute of Arctic and Alpine Research (INSTAAR), Version: 2018-09-24, Path: ftp://aftp.cmdl.noaa.gov/data/trace_gases/ch4c13/flask/, 2018.

Widory, D.: Combustibles, fuels and their combustion products: A view through carbon isotopes, Combust. Theory Model., 10, 831-841, https://doi.org/10.1080/13647830600720264, 2006.

Wietzel, J. B., and Schmidt, M.: Methane emission mapping and quantification in two medium-sized cities in Germany: Heidelberg and Schwetzingen, Atmos. Environ.: X, 20, https://doi.org/10.1016/j.aeaoa.2023.100228, 2023.

WMO 2020: 20th WMO/IAEA Meeting on Carbon Dioxide, Other Greenhouse Gases and Related Measurement Techniques (GGMT-2019), Jeju Island, South Korea 2–5 September 2019. GAW Report No. 255, https://library.wmo.int/idurl/4/57135, 2020.

York, D., Evensen, N. M., Martinez, M. L., and Delgado, J. D.: Unified equations for the slope, intercept, and standard errors of the best straight line, Am. J. Phys., 72, 367-375, https://doi.org/10.1119/1.1632486, 2004.

Zazzeri, G., Lowry, D., Fisher, R. E., France, J. L., Lanoisellé, M., and Nisbet, E. G.: Plume mapping and isotopic characterisation of anthropogenic methane sources, Atmos. Environ., 110, 151-162, https://doi.org/10.1016/j.atmosenv.2015.03.029, 2015.

700 Zazzeri, G., Lowry, D., Fisher, R. E., France, J. L., Lanoisellé, M., Grimmond, C. S. B. and Nisbet, E. G.: Evaluating methane inventories by isotopic analysis in the London region, Sci. Rep. 7, 4854, https://doi.org/10.1038/s41598-017-04802-6, 2017.

Zobitz, J., Keener, J., Schnyder, H. and Bowling, D.: Sensitivity analysis and quantification of uncertainty for isotopic mixing relationships in carbon cycle research, Agricultural and Forest Meteorology, 136 (1) (2006) 56-75, ISSN 0168-1923, http://doi.org/10.1016/j.agrformet.2006.01.003, 2006.
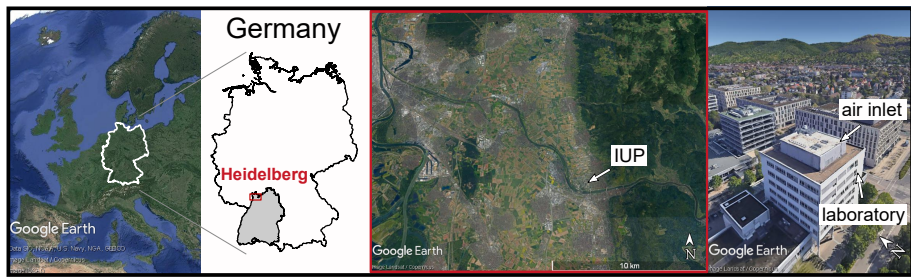
Figure 1. Location of the measurement station in Heidelberg at the Institute of Environmental Physics (IUP - Institut für Umweltphysik) (map data ~~on~~ from © Google Earth).
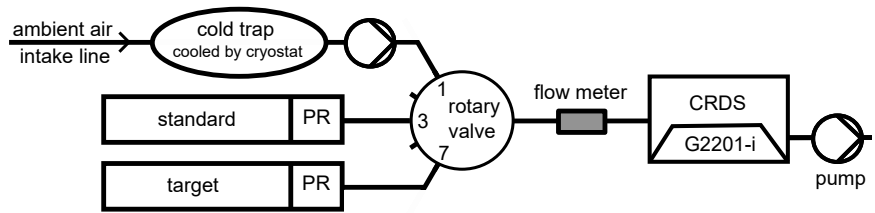
Figure 2. Experimental setup to measure CH_4 mole fraction and $\delta(^{13}CH_4)$ in ambient air in Heidelberg.
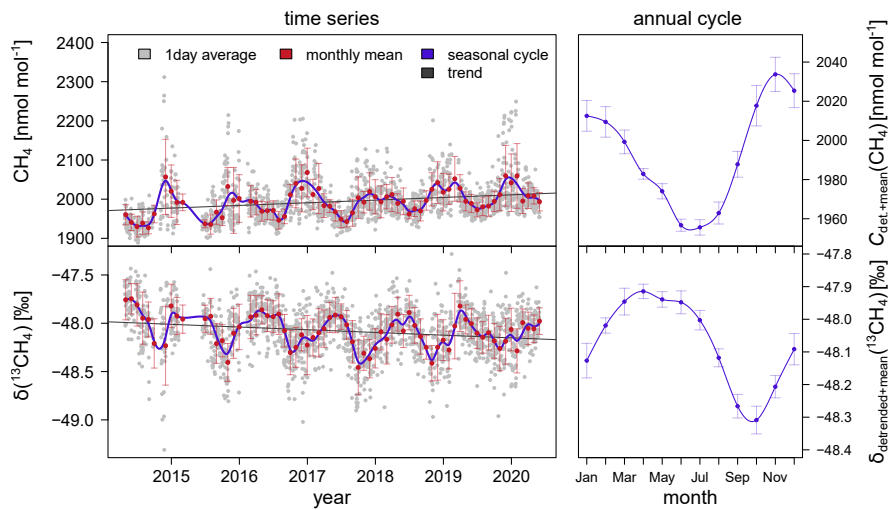
Figure 3. Atmospheric CH_4 mole fraction and $\delta(^{13}CH_4)$ measured in Heidelberg and corresponding annual cycles. The monthly mean values and standard deviation (red) are calculated from the daily averages (grey). The mean annual cycle with the standard errors are shown in blue. Note that the y-axis ranges are not the same for the left and right panels.
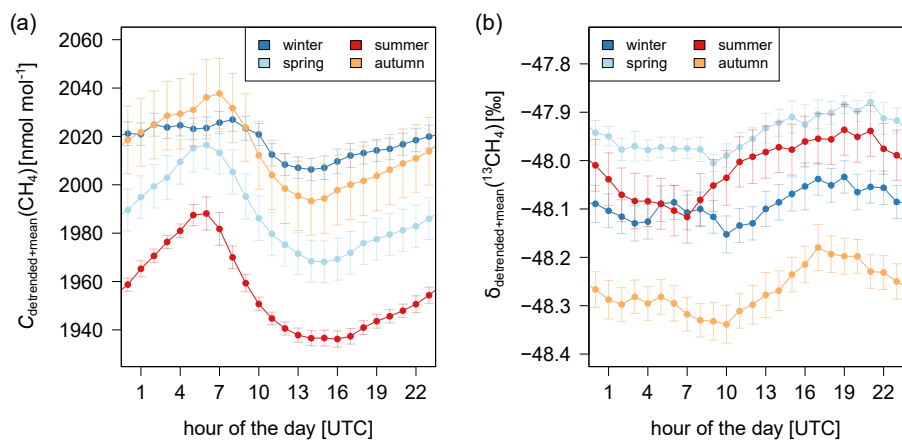
Figure 4. Diurnal cycles of CH$_4$ (a) and $\delta(^{13}\text{CH}_4)$ (b) in Heidelberg. For each season the diurnal cycles of each month, which are detrended by subtracting the diurnal mean, are averaged and the mean CH$_4$ mole fraction or $\delta(^{13}\text{CH}_4)$ value for each season is added.
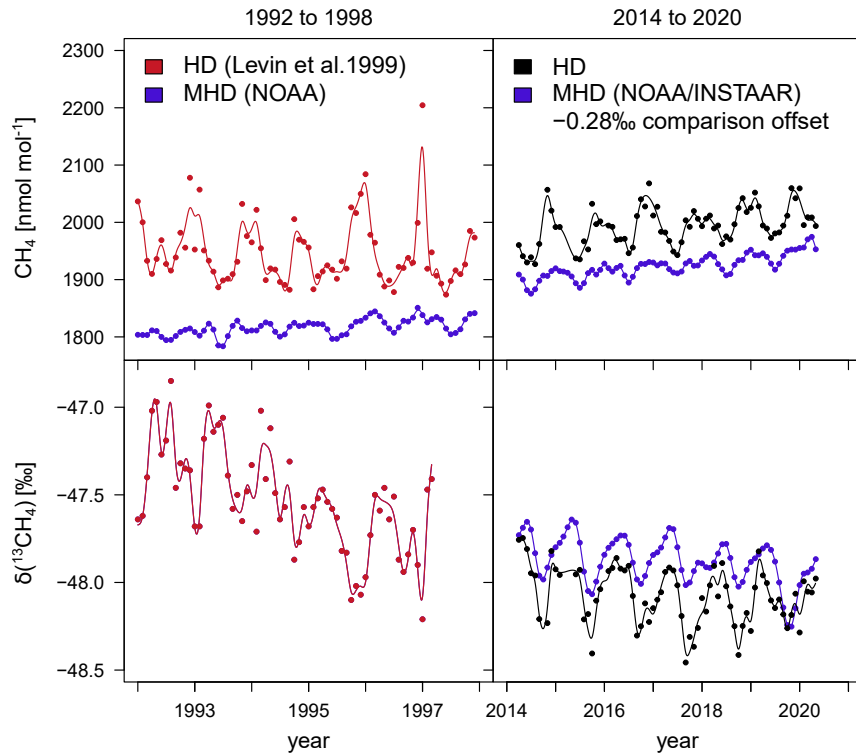
Figure 5. CH$_4$ mole fraction and $\delta(^{13}CH_4)$ in Heidelberg from 1992 to 1998 (Levin et al., 1999) and between 2014 and 2021. In addition, measurements done at the marine background station Mace Head (Lan et al., 2022; Michel et al., 2022) are shown in blue.
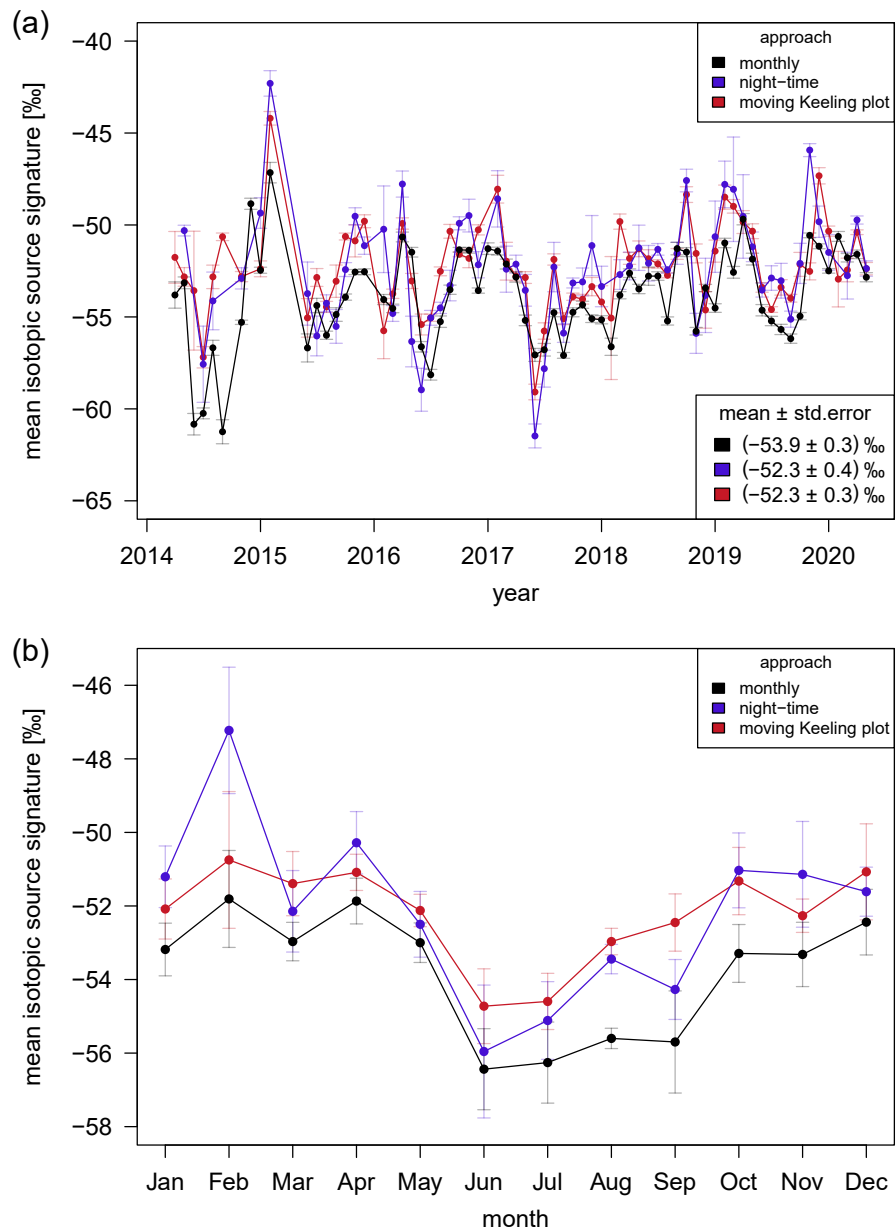
Figure 6. The monthly averages (a) and the annual cycle (b) of the mean $\delta^{13}C$ isotopic carbon source signatures of CH_4 in the catchment area of Heidelberg between April 2014 and May 2020. The monthly (black), the night-time (blue) and the moving ~~Miller-Tans~~ Keeling plot (red) approach are used for the determination. The error bars corresponds to the standards deviations.
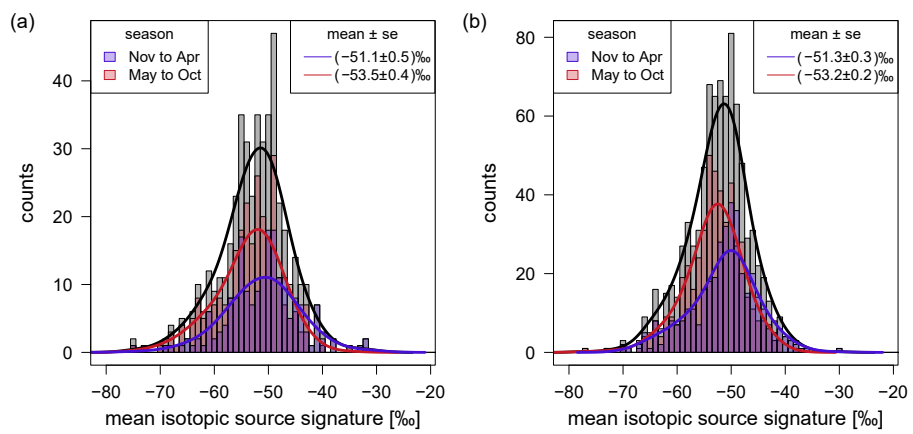
Figure 7. Frequency distribution of the determined mean CH_4 isotopic source signatures of individual nights (a) or ~~events~~ daily averages (b) in the catchment area of Heidelberg.
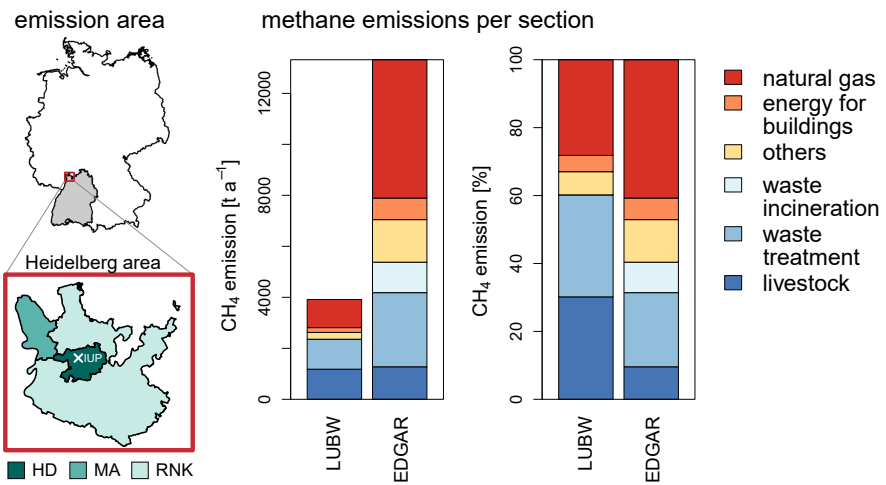
Figure 8. CH$_4$ emissions and relative proportion of different source categories reported by LUBW (LUBW, 2016) and calculated from EDGAR v6.0 (Crippa et al., 2021) data for the Heidelberg area, which includes the cities of Heidelberg (HD) and Mannheim (MA) as well as the county Rhein-Neckar-Kreis (RNK).

Table 1. Isotopic ^{13}C signatures of different CH_4 sources based on measured values in the catchment area of Heidelberg and literature: (1) Hoheisel et al., 2019, (2) Levin et al., 1993, (3) Sherwood et al., 2017, (4) Widory et al., 2006 (for $\delta(^{13}CO_2)$), (5) Menoud et al., 2021 and (6) Zazzeri et al., 2017.

| Sector	Source	Isotopic ^{13}C signature [‰]
livestock farming	ruminants[1]	-63.9 ± 1.3
solid waste landfills	landfill[1]	-58.7 ± 3.3
waste water treatment	waste water treatment plant[1]	-52.5 ± 1.4
exploitation of oil and coal	coal from Europe and Russia[3]	-46.6 ± 6.4
gas distribution	natural gas[1]	-43.3 ± 0.8
waste incineration	waste incineration[4]	-33.2 ± 4.6
energy for buildings	non-industrial combustion[5]	~~-31.1~~-32.1
industrial emissions	combustion (industrial)[6]	-25
road transport	cars[2]	-22.8
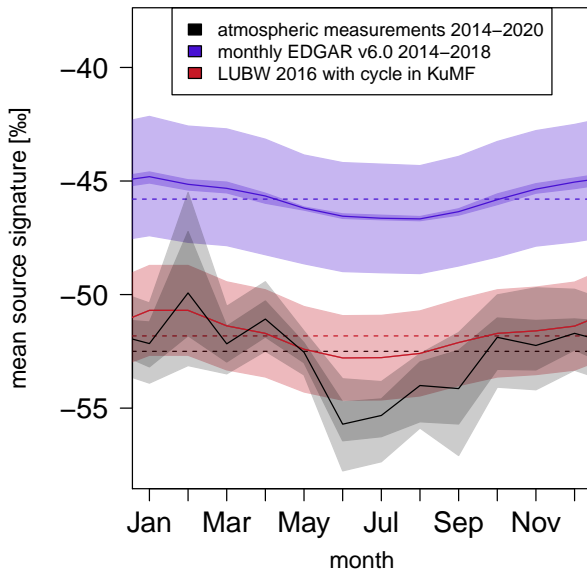
Figure 9. Annual variability in the monthly mean CH$_4$ isotopic source signatures calculated with emission inventories and atmospheric measurements for the Heidelberg area. The light blue and red areas for EDGAR v6.0 (Crippa et al., 2021) and LUBW (LUBW, 2016) corresponds to errors in the applied source signatures and the dark blue area for EDGAR v6.0 shows differences in the CH$_4$ isotopic source signatures for all years between 2014 and 2018. The dark grey area corresponds to the results for atmospheric measurements from the different approaches and the light grey area includes errors, too.

Table A1. CH_4 mole fraction and isotopic ratio of the two calibration gases used to calibrate the ambient air measurements carried out in Heidelberg.

| period of use	CH_4 [nmol mol^{-1}]	$\delta(^{13}CH_4)$ [‰]
up to August 2019	1934.5 ± 0.1	-47.83 ± 0.05
from August 2019	2003.6 ± 0.4	-48.10 ± 0.07
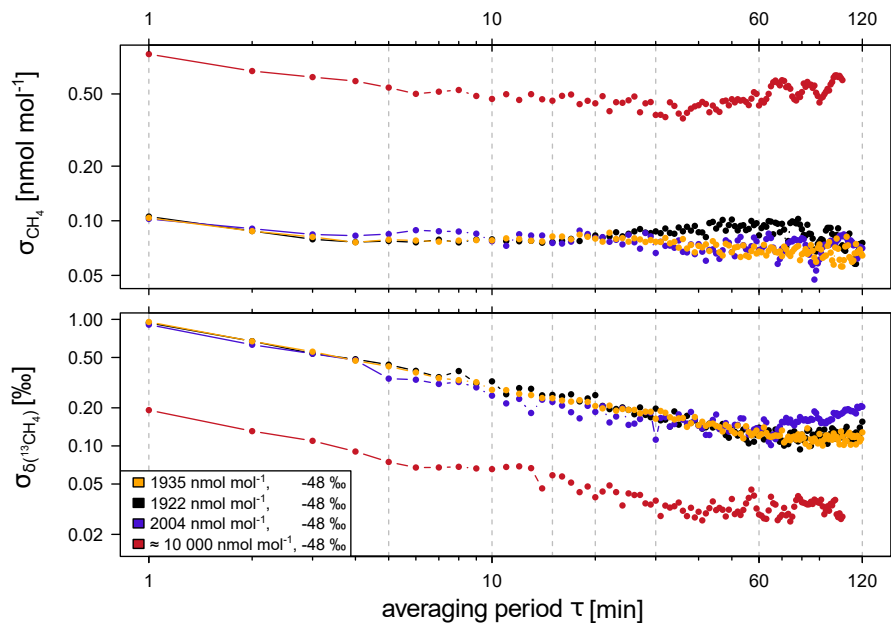
Figure A1. Allan standard deviations for CH_4 mole fraction and $\delta\left(^{13}CH_4\right)$ determined for the CRDS G2201-i analyser and different CH_4 mole fractions and isotope ratios. The Allan standard deviations are based on measurements from 2013 (orange) and 2019 (black, blue, red).
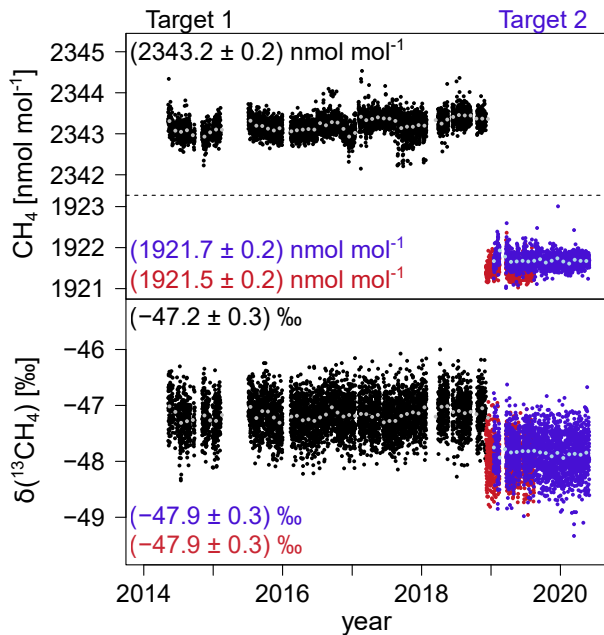
Figure A2. Calibrated CH_4 mole fractions and $\delta(^{13}CH_4)$ values of the target cylinder measurements. Target 1 (calibrated with calibration cylinder 1) is shown in black and Target 2 (calibrated with calibration cylinder 2) in blue. The grey and light blue data points correspond to the monthly average values. For quality control, Target 2 was additionally calibrated with calibration cylinder 1 and is shown here in red.

Table A2. $\delta(^{13}CH_4)$ measurements of six intercomparison cylinders. The $\delta(^{13}CH_4)$ values determined by MPI-BGC are taken from Umezawa et al. (2018) and are compared with our results. The difference of the multiple measurements is shown in parenthesis and the uncertainty of the average difference is given as the standard error of the mean.

sample ID (collection date)	analysis date MPI-BGC	analysis date UHEI-Pic	$\delta(^{13}CH_4)$ MPI-BGC [‰]	$\delta(^{13}CH_4)$ UHEI-Pic [‰]	difference UHEI−MPI [‰]
GvN 88/20 (Jul 1988)	Jul 2013	May 2018 & May 2019	−47.66 (0.07, N= 2)	−47.60 (0.29, N= 3)	+0.06
GvN 92/12 (May 1992)	Jun 2013	May 2018 & May 2019	−47.40 (0.04, N= 2)	−47.61 (0.19, N= 4)	−0.21
GvN 96/03 (Feb 1996)	Jun 2013	May 2018 & Apr 2019	−47.18 (0.26, N= 2)	−47.07 (0.23, N= 3)	+0.11
GvN 99/14 (Dec 1999)	Jul 2013	Jun 2018 & Apr 2019	−47.23 (0.16, N= 2)	−47.13 (0.02, N= 2)	+0.10
GvN 06/14 (Sep 2006)	Jul 2013	May 2019 & Feb 2020	−47.19 (0.09, N= 2)	−47.26 (0.23, N= 3)	−0.07
GvN 08/03 (Mar 2008)	Jun 2013	Feb 2020	−47.35 (0.05, N= 2)	−47.24 (0.37, N= 2)	+0.11
average					$(+0.02 \pm 0.05)‰$